NASA Contractor Report 3868

Unsteady Analysis of Rotor Blade Tip Flow

B. Maskew and B. M. Rao
Analytical Methods, Inc.
Redmond, Washington

Prepared for
Langley Research Center
under Contract NAS1-15472

National Aeronautics
and Space Administration

**Scientific and Technical
Information Branch**

1985

TABLE OF CONTENTS

LIST OF FIGURES

LIST OF FIGURES (CONCLUDED)

LIST OF TABLES

1.0 INTRODUCTION

The following is the final report on the development of two computer programs, VSAERO-TS and VSAERO-H, for calculating the unsteady subsonic aerodynamic characteristics of arbitrarily-shaped wings oscillating in pitch. The work is part of an investigation of the combined effects of unsteady motion and planform shape on the aerodynamic loading of helicopter blades. Four blade-tip planforms were evaluated; these include a rectangular, a tapered, a swept and an ogee shape, Figure 1. Each blade is considered as a semispan wing oscillating in pitch; i.e., blade rotation is excluded at this time.

Experimental data have been measured on the four blades by the Institut fur Aeroelastik in the DFVLR 3 x 3 m tunnel in Gottingen, West Germany. Correlations between calculated and measured unsteady chordwise pressure distributions were presented in Reference 1. The present report describes the theoretical background to the methods and includes results from parametric studies.

During the correlation study the time-stepping program had difficulties with the tapered and ogee planforms and also with the tip vortex effects. Modifications have now been installed in the VSAERO-TS program to overcome these difficulties and are discussed in this report.

Both programs, VSAERO-TS and VSAERO-H, have a common basis (Figure 2) in program VSAERO, which is under continued development (2) through (6) for the analysis of steady, non-linear aerodynamic characteristics of arbitrary configurations with extensive vortex separations. Program VSAERO-TS is a time-stepping analysis capable of treating large amplitude motions while program VSAERO-H uses a harmonic wake and small amplitude assumptions. VSAERO-H, therefore, is basically similar to Geissler's method (7); the main difference is that VSAERO-H uses an internal Dirichlet boundary condition to establish a unique relationship between the source and doublet singularity distributions.

The basis of these computer programs is a surface singularity panel method which uses quadrilateral panels on which doublet and source singularities are distributed in a piecewise constant form. The panel source values are directly determined by the external Neumann boundary conditions controlling the normal component of the local resultant flow; the doublet values are solved after imposing the internal Dirichlet boundary condition of zero perturbation potential at the center (underside) of all the panels simultaneously. Surface perturbation velocities are obtained from the gradient of the doublet solution, while field velocities are obtained by direction summation of all singularity contributions. The details of the mathematical formulation are

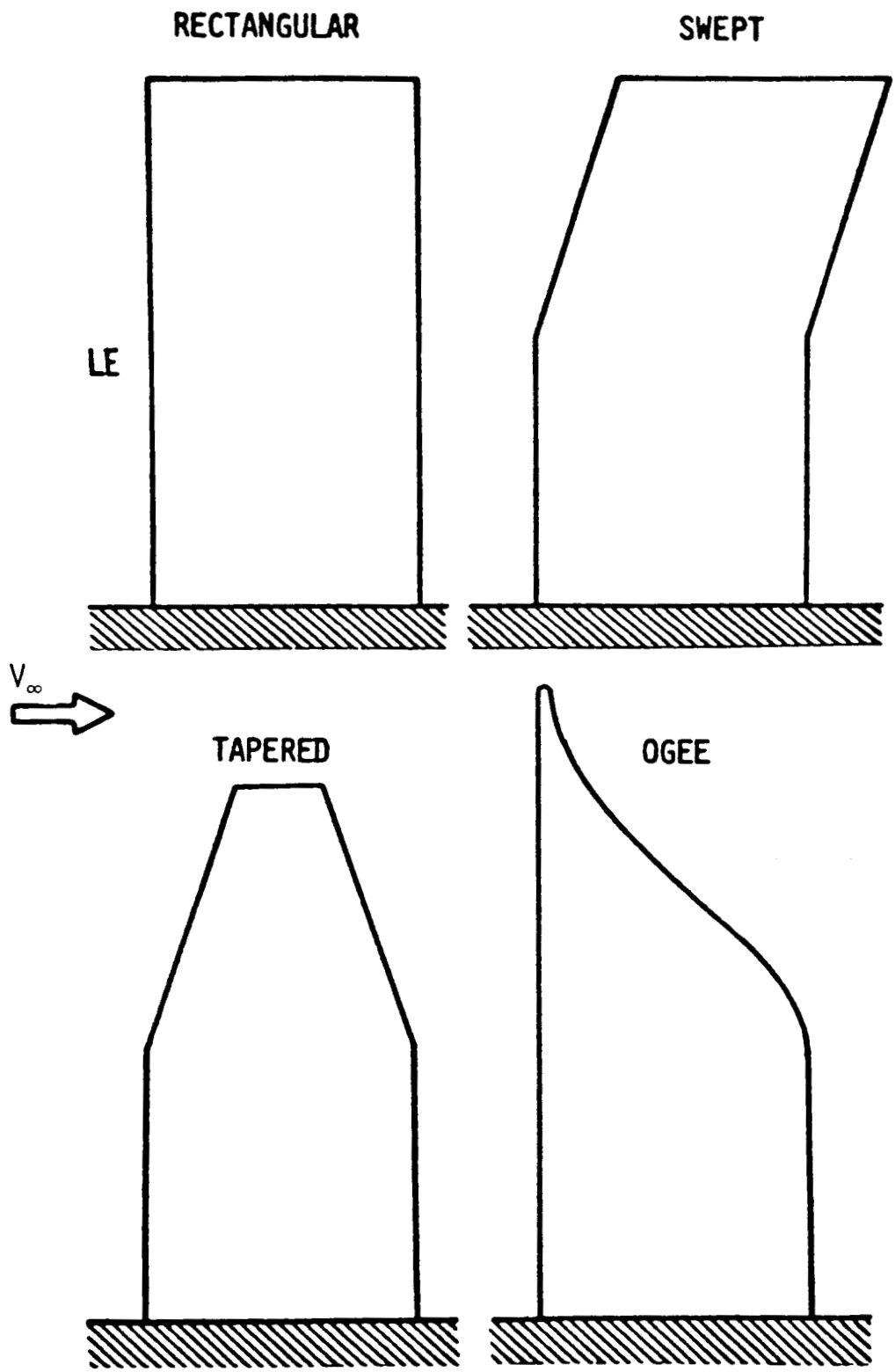

Figure 1. Planforms for Unsteady Blade-Tip Study.

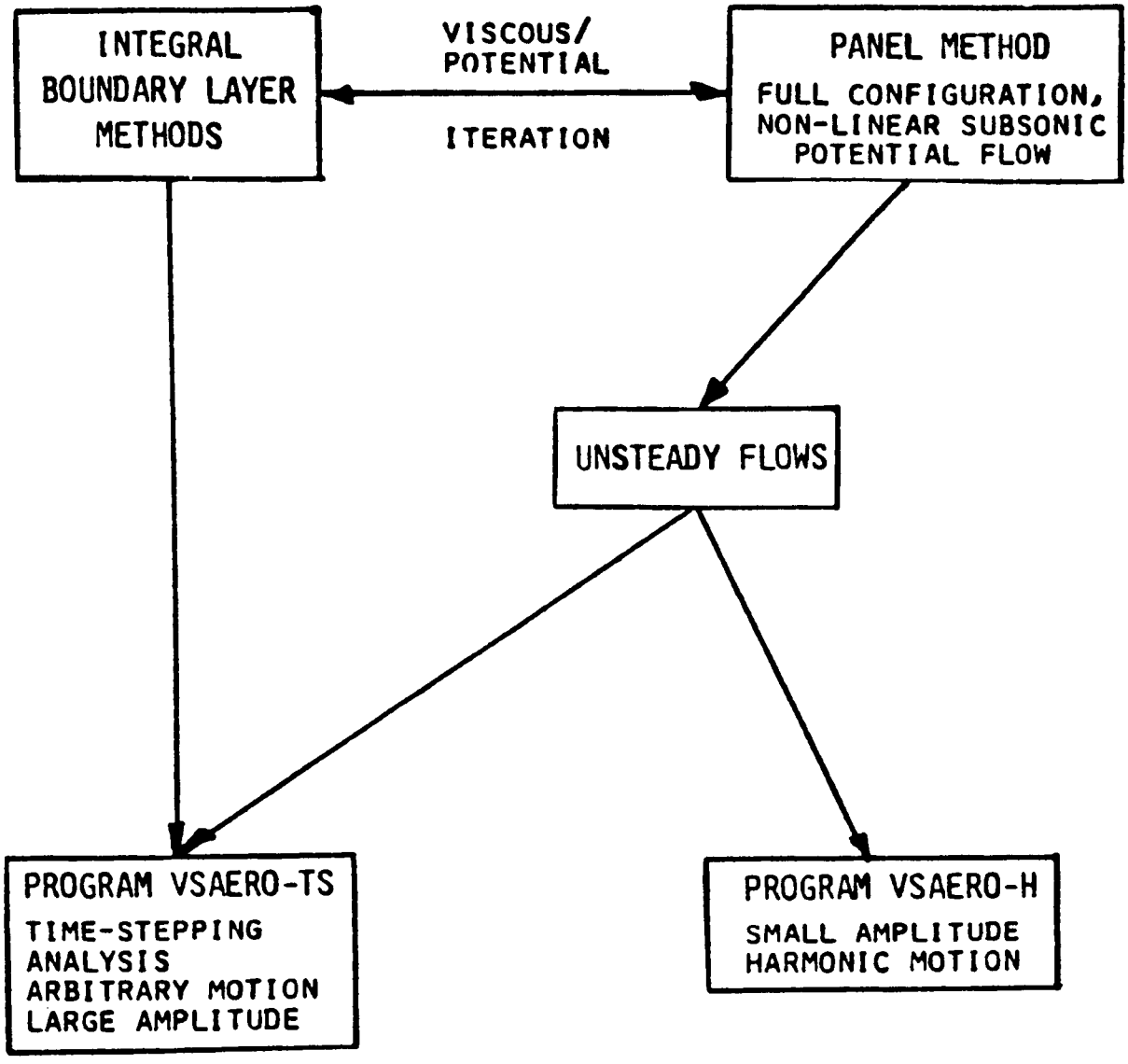

Figure 2. VSAERO Unsteady Program Development.

presented in Section 3, while the numerical procedure for obtaining the unsteady pressure distribution, forces and moments is presented in Section 4.

In Section 5, the viscous/potential flow iterative scheme is discussed. This capability comes from the basic VSAERO program (Figure 2) and is applied here in VSAERO-TS at the mean angle of attack for the purpose of establishing the extent of tip-edge separation. A typical calculation for steady flow predicting the tip flow is presented for the rectangular tip.

In Section 6, a discussion on the convergence characteristics of the VSAERO-H wake integrals is presented. The two doublet distribution models for representing the wake are discussed.

In Section 7, several typical results and parametric studies are presented. Included here are cases run after the correlation studies (1) and following modifications to the VSAERO-TS program. The recent changes in the shedding model have significantly improved the treatment of the tapered and ogee planforms and additions to the wake influence coefficient evaluation for highly skewed panels have improved the treatment of the roll-up region near the tip vortex. A brief summary and conclusions are presented in Section 8.

2.0 NOTATION

B,C	Velocity potential influence coefficients for constant source and doublet distributions, respectively, on quadrilateral panels, Eq. (7)
c	Airfoil chord (m)
C_p	Pressure coefficient
C_L	Lift Coefficient
C_M	Pitching moment coefficient
E	Quantity in Eq. (7)
f	Frequency (Hertz)
h	Pitch axis unit vector
i,j,k	Orthogonal unit vector system defining the axes of the Cartesian coordinate system fixed relative to the blade, Figure 2
ℓ	Characteristic length, half mean chord (m)
N	Number of panels
n	Surface unit normal vector directed into the flow field
R	Position vector of a point relative to a point on the pitch axis
S	Blade surface
s	Surface distance (m)
t	Time (sec)
T	Normalized time, $V_\infty t/\ell$
V	Velocity (m/sec)
v	Perturbation velocity (m/sec)
W	Wake surface
x,y,z	Cartesian coordinates in the blade-fixed frame

α	Onset flow incidence measured in the blade-fixed frame, Figure 2
$\dot{\alpha}$	Rate of change of α
α_o	Mean angle of attack
α_i	Oscillation amplitude (mean to peak)
Δ	Finite increment
η	Spanwise location normalized by semispan
μ	Doublet strength
Φ	Total velocity potential
ϕ	Perturbation velocity potential
σ	Source strength
σ_R, σ_M	Source components due to unit pitch rotation and unit translation, respectively, Eq. (7)
ω	Reduced Frequency
∇	Gradient operator

Subscripts

J,K	Values on panels, J,K, respectively
U,L	Upper, lower
R,I	Real, imaginary components normalized by α_i
W	Wake
∞	Reference onset condition

3.0 MATHEMATICAL MODEL OVERVIEW

3.1 Formulation

The general arrangement of a configuration is shown in Figure 3 and is described in terms of a blade-fixed GLOBAL COORDINATE SYSTEM referred to as the G.C.S. The configuration is immersed in a uniform onset flow, V_∞, with velocity potential ϕ_∞. Potential flow is assumed to exist both inside and outside the boundaries of the configuration. In the external flow field (i.e., the one of interest) the total velocity potential, Φ, is the sum of the onset flow potential, ϕ_∞, and the perturbation potential, ϕ. Similarly, the total velocity potential inside the configuration is Φ_i. For the present description, the wake surfaces are assumed to have vanishing thickness with zero entrainment.

After applying Green's Theorem to the inner and outer regions and combining the resulting expressions, the velocity potential at a point P on the inside surface can be written

$$4\pi\Phi_p = \iint_{S-P} (\Phi - \Phi_i)\mathbf{n} \cdot \nabla\left(\frac{1}{r}\right) dS - 2\pi(\Phi - \Phi_i)_p + \iint_W (\Phi_U - \Phi_L)\mathbf{n} \cdot \nabla\left(\frac{1}{r}\right) dW + \iint_S \frac{1}{r}\,\mathbf{n} \cdot (\nabla\Phi_i - \nabla\Phi)\, dS + 4\pi\phi_{\infty p} \qquad (1)$$

where r is the length of the vector from the surface element to the point, P, and S-P signifies that the point, P, is excluded from the surface integral. $\Phi_U - \Phi_L$ is the local jump in potential across the wake surface, W. Equation (1) gives the total potential at the interior point, P, as the sum of perturbation potentials due to a normal doublet distribution of strength $(\Phi - \Phi_i)$ on S and $(\Phi_U - \Phi_L)$ on W, respectively, and a source distribution of strength, $\mathbf{n} \cdot (\nabla\Phi_i - \nabla\Phi)$ on S. The potential for the uniform onset flow, ϕ_∞, is also included.

In principle, an infinite number of combinations of doublet and source distribution will give the same external flow field, but different internal flow fields. To render a unique combination of singularities, either one of the singularity distributions must be specified (e.g., $\sigma = 0$ in the doublet-only formulation) or, as in the present case, the internal flow must be specified. There are several reasonable options for the internal potential flow. One of the most convenient options is to set $\Phi_i = \phi_\infty$. This internal Dirichlet boundary condition gives zero perturbation to the onset flow inside the configuration.

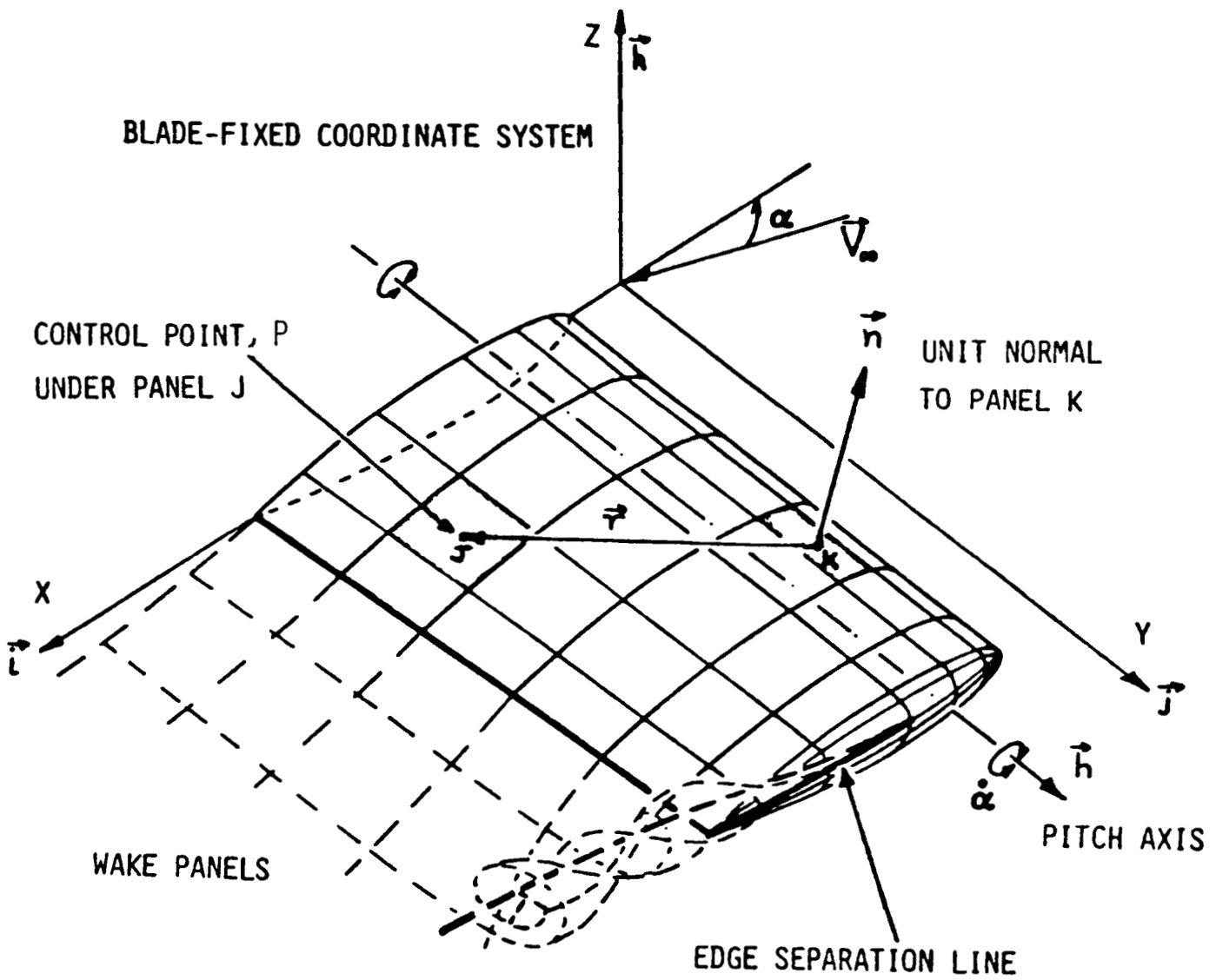

Figure 3. General Arrangement of the Configuration.

Equation (1) becomes

$$0 = \iint_{S-P} \phi \mathbf{n} \cdot \nabla \left(\frac{1}{r}\right) dS - 2\pi\phi_p + \iint_{W} (\Phi_U - \Phi_L)\mathbf{n} \cdot \nabla \left(\frac{1}{r}\right) dW - \iint_{S} \frac{1}{r} \mathbf{n} \cdot \nabla\phi \qquad (2)$$

where ϕ, the perturbation potential in the flow field has been substituted for $\Phi - \Phi_\infty$.

The first two terms in Eq. (2) give the perturbation potential due to a distribution of normal doublets of strength, ϕ, on the configuration surface, S. Similarly, the third term represents a doublet distribution of strength, $\Phi_U - \Phi_L$, on the wake and the fourth term represents a source distribution on strength $\sigma = \mathbf{n} \cdot \nabla\phi$ on the configuration surface.

For the problem of analyzing the flow about a given configuration geometry, the doublet distribution, ϕ, is the unknown while the source distribution is determined directly by the external Neumann boundary conditions; i.e., the source term in Eq. (2) can be evaluated directly from the condition of no flow penetration at the surface. The flow velocity relative to the blade-fixed frame is

$$\mathbf{V} = \mathbf{v} + \mathbf{V}_\infty - \dot{\alpha}\mathbf{h} \wedge \mathbf{R}, \qquad (3)$$

where the perturbation velocity, $\mathbf{v} = -\nabla\phi$.

For zero penetration, $\mathbf{V} \cdot \mathbf{n} = 0$. Hence,

$$\mathbf{n} \cdot \nabla\phi = \mathbf{n} \cdot \mathbf{V}_\infty - \dot{\alpha}\mathbf{n} \cdot \mathbf{h} \wedge \mathbf{R},$$

and Eq. (2) becomes

$$0 = \iint_{S-P} \phi\, \mathbf{n} \cdot \nabla \left(\frac{1}{r}\right) dS - 2\pi\phi_p + \iint_{W} \left(\phi_U - \phi_L\right) \mathbf{n} \cdot \nabla \left(\frac{1}{r}\right) dW - \iint_{S} \frac{1}{r} \left(\mathbf{n} \cdot \mathbf{V}_\infty - \dot{\alpha}\, \mathbf{n} \cdot \mathbf{h} \wedge \mathbf{R}\right) dS \qquad (4)$$

This is the basic equation of the method. It is solved for the unknown surface perturbation potential, D, or surface doublet distribution, at a number of time steps as the blade proceeds through pitch oscillations. The wake surface is relocated at the end of each step to satisfy the zero load condition. The doublet distribution, $\phi_U - \phi_L$, on the wake is related to conditions at the trailing edge in the steady case, while in the unsteady, time-stepping mode, the wake doublet values and wake location are known form solutions at earlier time steps. In the unsteady mode the Kutta condition

$$\frac{\partial \mu}{\partial t} + V \frac{\partial \mu}{\partial s} = 0 \tag{5}$$

is satisfied at points along the wake separation line at each time step.

At each time step the flow solution is determined with reference to the blade-fixed frame. The incompressible pressure coefficient is, therefore, given by

$$C_p = \left(V_s^2 - V^2 + 2 \frac{\partial \mu}{\partial t}\right)/V_\infty^2 \tag{6}$$

where $\mathbf{V}_s = \dot{\alpha}\mathbf{h} \wedge \mathbf{R} - \mathbf{V}_\infty$ is the instantaneous velocity of a point on the surface relative to a stationary reference frame, and $\mathbf{V}$ is given by Eq. (3).

Although the modulus of $\mathbf{V}_\infty$ is constant in the present calculations, its components in the blade-fixed frame are functions of time, with the instantaneous angle of attack

$$\alpha(t) = \alpha_o + \alpha_i \sin(pt)$$

Hence, the instantaneous rotation rate about the pitch axis is

$$\dot{\alpha}(t) = \alpha_i p \cos(pt).$$

In the case of harmonic (unsteady) flow, the motion and the velocities are assumed to undergo a periodic variation. For example, the doublet strength, $\mu = \mu_e^{ipt} = \mu_e^{i\omega T}$, where μ is the amplitude, ℓ, a reference length (usually semi-chord); $\omega = p\ell/V_\infty$ (reduced frequency); and $T = tV_\infty/\ell$ (non-dimensional time). For harmonic flow, one solves for the amplitude of doublet strength (complex), taking into account its variation in the wake consistent with the unsteady Kutta condition.

4.0 NUMERICAL PROCEDURE

The numerical procedure to obtain the unsteady pressure distribution, forces and moments is shown in Figure 4. The surface of the blade is represented by planar quadrilateral panels over each of which the doublet and source distributions are assumed constant. The input data is assembled in three main parts: basic data, surface patch geometry description and basic wake geometry description. Also, automatic paneling routines are installed to simplify user input. Complete details of the input parameters, output description, a detailed diagram showing the connections between subroutines in the code and user notes for the geometry description are presented in Reference 8.

Equation (4) is satisfied simultaneously at a point at the center of each panel. If there are N panels representing the blade surface, Eq. (4) becomes:

$$\sum_{\substack{k=1 \\ K \neq J}}^{N} \left\{ \mu_K \, C_{JK} \right\} - 2\pi\mu_J + E_J = 0; \qquad J=1,N \tag{7}$$

where μ_K is the unknown doublet value on panel K. (Note: $\mu_K = \phi_K/4\pi$.)

$$E_J = \sum_{K=1}^{N_W} \left\{ \mu_{W_K} \, C_{JK} \right\} + \dot{\alpha}\sigma_{R_J} - \mathbf{V}_\infty \cdot \sigma_{M_J}$$

where N_W, the number of panels in the wake, varies with time and $\dot{\alpha}$ and $\mathbf{V}_\infty$ take their instantaneous values at each time step.

$$\sigma_{R_J} = \left\{ \sum_{K=1}^{N} \mathbf{h} \wedge \mathbf{R}_K \cdot \mathbf{n}_k \, B_{JK} \right\} / 4\pi$$

is the source distribution due to blade rotation about the pitch axis, and

$$\sigma_{M_J} = \left\{ \sum_{K=1}^{N} \mathbf{n}_K \, B_{JK} \right\} / 4\pi$$

are the components of a three-part source distribution due to the relative translation of the blade and the onset flow. (Note: in the present symmetrical case the y-component is zero.)

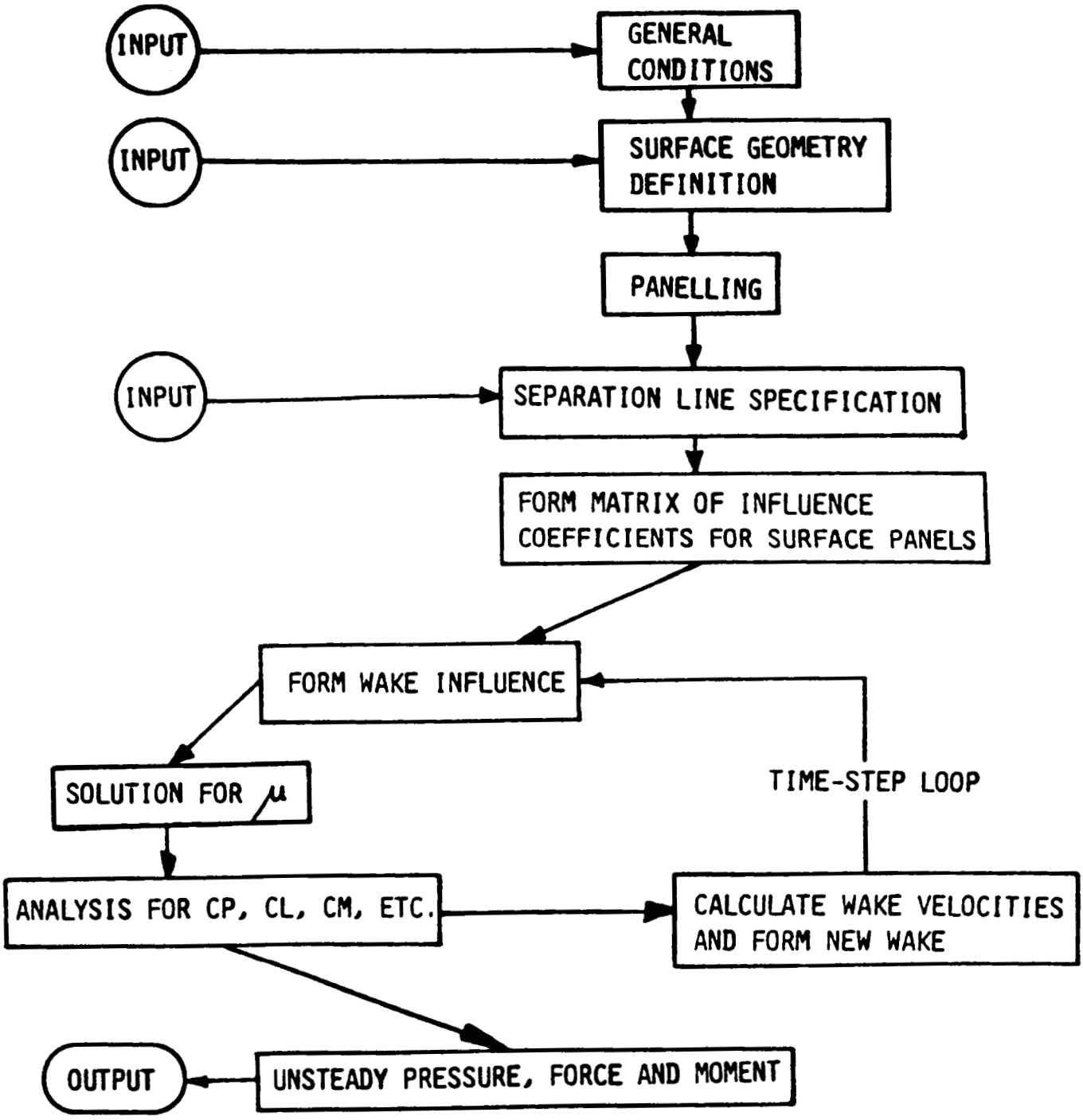

Figure 4. Flow Diagram for the Method.

The quantities, B_{JK} and C_{JK}, are the velocity potential influence coefficients for the constant source and doublet distributions, respectively, on panel K acting on the control point on panel J. These include contributions from the image panel in this case. Expressions for these influence coefficients have been given by Morino (9) based on hyperbolic paraboloidal panels. Slightly different expressions are installed in the present code based on planar panels.

When the influence coefficient matrix has been assembled, Eq. (7) is solved by a direct method for $N \leq 320$ and by an iterative method for $N > 320$.

The surface pressure distribution is calculated using Eq. (6). The surface gradient of μ is evaluated on each panel by differentiating a two-way parabolic fit through the doublet values on the panel and its four immediate neighbors. At the separation lines a simple differencing is applied for the gradients approaching the separation line.

The gradient of ϕ with respect to time is evaluated by central differencing over two time steps; i.e.,

$$\left(\frac{\partial \phi}{\partial t}\right)^{t-\Delta t} = \left(\phi^{t} - \phi^{t-2\Delta t}\right)/2\Delta t.$$

The real and imaginary pressures are obtained by Fourier analysis for the first harmonic based on solutions over a complete cycle. The calculations start with incidence α_o and a regular (i.e., steady) wake. Two iterations are performed to render the wake force free. Based on several test cases, two iterations proved to be adequate. An oscillatory doublet component based on a linearized solution is then superimposed along each wake line before starting the time-step mode. Time-step calculations proceed over a half cycle before applying the Fourier analysis. This was done to eliminate the transient effects of the initial calculation.

At each time step a new panel is formed at the head of each column of wake panels and all the existing wake panel corner points are convected downstream at the computed local velocity. The doublet value on each new panel is based on the conditions at the separation line and satisfies the Kutta condition, Eq. (5). It is assumed that the shedding occurs at constant vorticity over the time interval, Δt. In this way the doublet strength, $\mu_W^{t+\Delta t}$, on the new wake panel is related to the strength, μ_W^{t}, of the previous wake panel at the trailing edge by

$$\mu_W^{t+\Delta t} = 2\mu_T^{t} - \mu_W^{t}$$

where μ_T^{t} is the resultant doublet value at the separation line.

Preliminary tests of the time-stepping calculation showed some sensitivity to time-step size relative to the local panel size at the trailing edge on each strip. In order to alleviate this a scheme was developed in the program whereby the x-wise location of the wake panels were fixed for all time by the user. Thus, at the outset of a calculation the user specifies a set of x-stations as locations of vertical cross-flow planes which will contain wake panel corner points, Figure 5. In principle, the planes can be located with a reasonable relationship to wake shedding panels at the blade trailing edge. The plane spacing can be made dense near the blade and can be opened out with increasing distance downstream. At each time step points on the present wake are first transported a small distance according to the local velocity and a time-step size; the NUWAKE routine then interpolates (using a biquadratic scheme) along each line and reforms the wake panel corner points--and the wake panel doublet values--in the user-specified wake-grid-plane system, Figure 6. This scheme alleviates the sensitivity to time-step size and also leads to a more effective use of a limited number of wake panels. Initially (1) the NUWAKE model had some difficulties in treating the tapered and ogee planforms, especially at the smaller reduced frequencies. The scheme has now been modified to give an improved trailing-edge doublet value (using an extrapolation from values at previous times) for interpolation in the immediate zone near the blade trailing edge. This has given a significant improvement in the behavior of the method relative to that in Reference 1, and good solutions are now obtained for the tapered tip and ogee planforms (Section 7).

In the preliminary version of the time-stepping program the wake panels had a piecewise constant doublet distribution. Later this was changed to a linear doublet distribution (i.e., constant vorticity) in the streamwise direction to provide a smoother representation of the vorticity. The influence coefficient for each panel is formulated for a planar surface and so a skewed panel is represented by a projected flat quadrilateral lying in the mean plane. Panels in the extreme roll-up region of the tip vortex are highly skewed and consequently the flat-panel influence coefficient representation leaves a large number of "holes" in the apparent vortex sheet surface. These holes cause a loss in the local induced effects on the blade tip surface and this leads to errors in the computed pressure distribution near to the tip vortex. The program has therefore been modified to treat each highly skewed panel as a pair of triangles, Figure 7. One of the diagonals of the quadrilateral is taken as the common side for the two triangles. In this way the influence coefficient evaluation now covers a continuous surface since the edges of skewed panels match up with their neighbors. The panels are still regarded as quadrilaterals as far as geometry, etc. is concerned; the triangle treatment is only applied in the near-field influence routine.

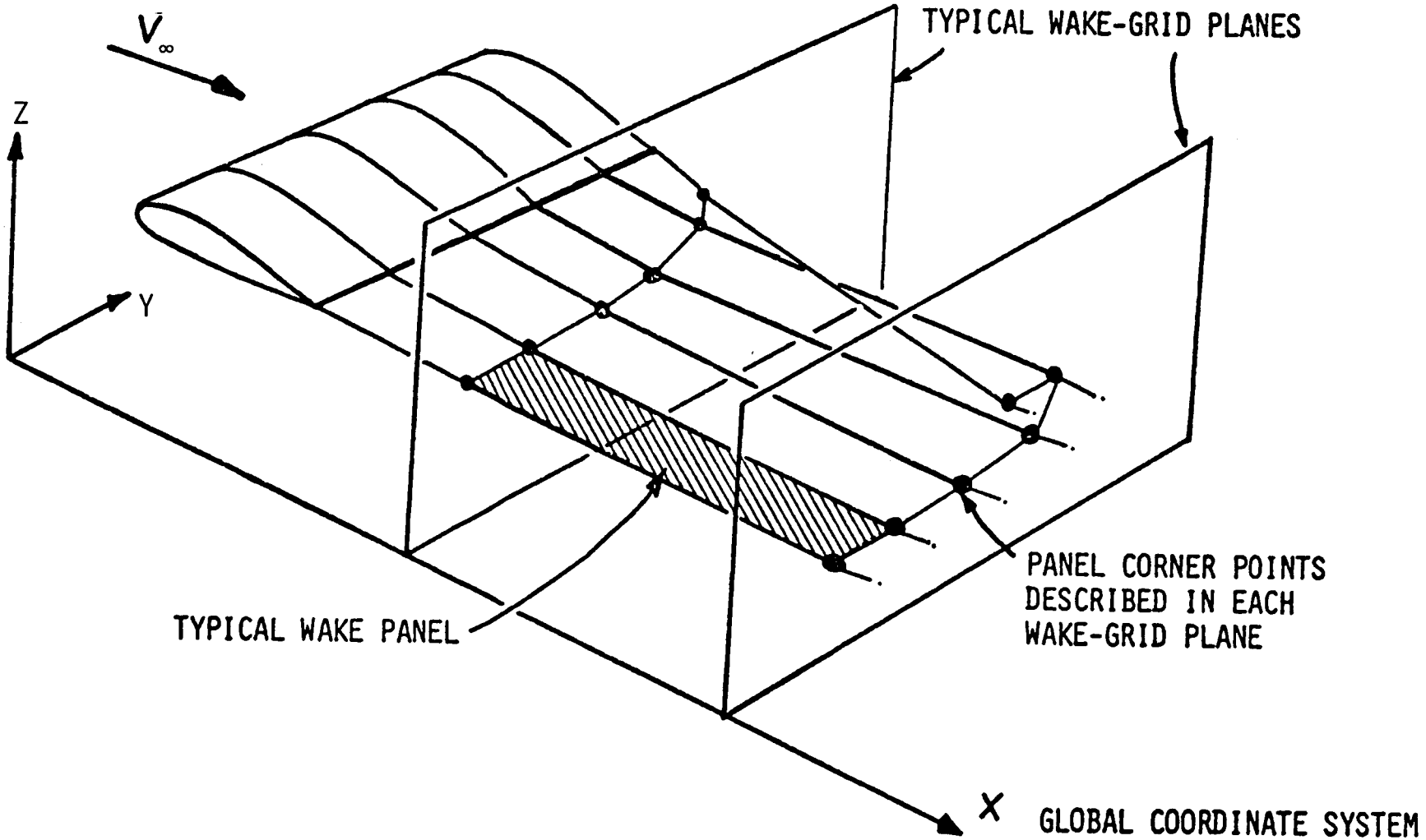

Figure 5. Wake-Grid-Plane Scheme.

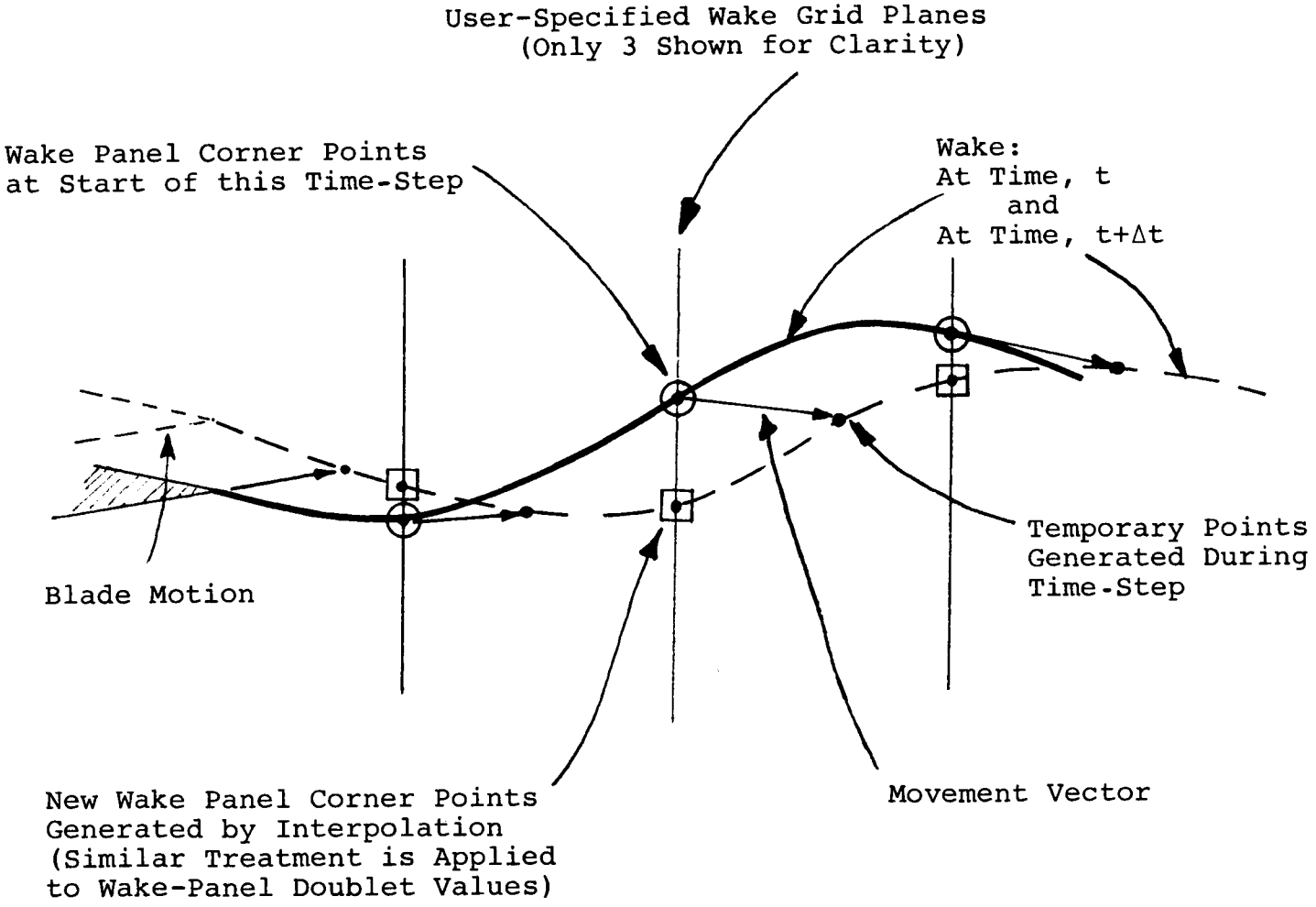

Figure 6. Section through Wake Model in VSAERO-TS (Schematic).

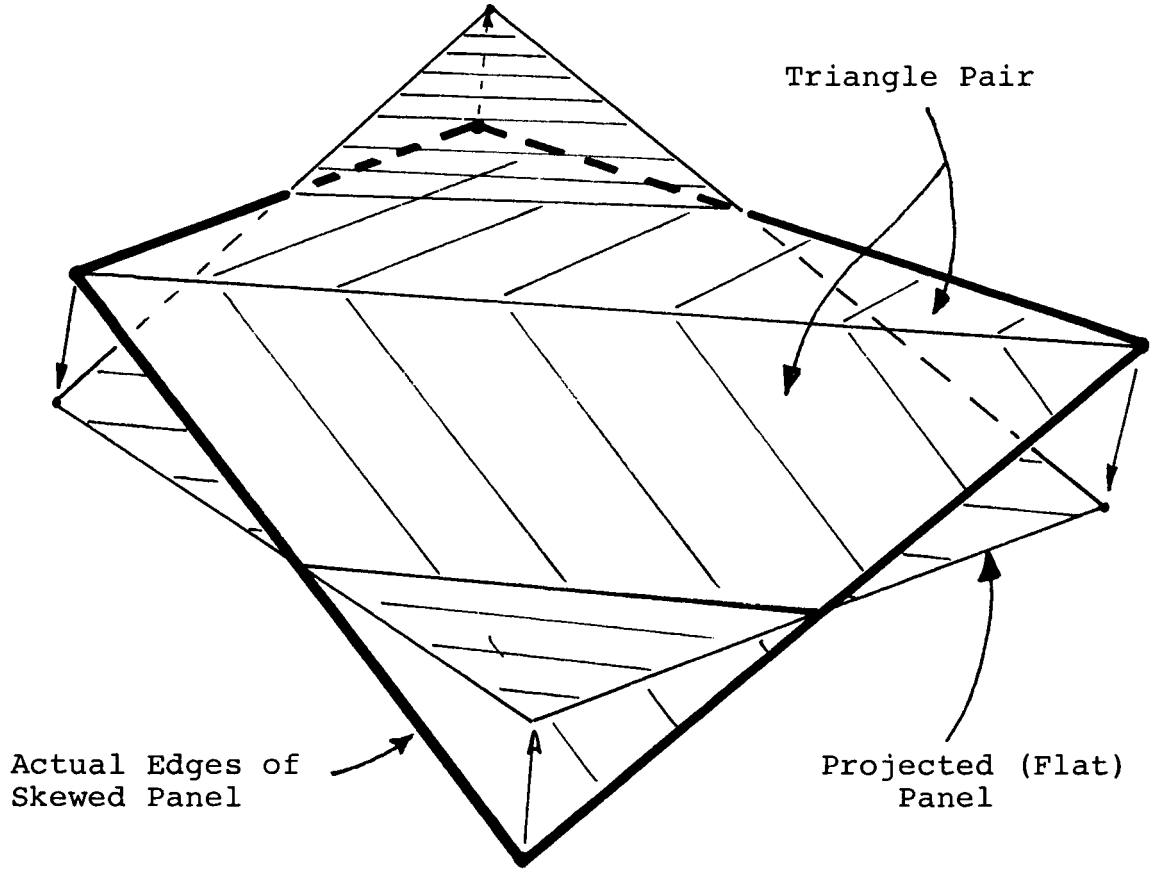

Figure 7. Treatment of Highly Skewed Wake Panels.

5.0 'VSAERO-TS': VISCOUS/POTENTIAL FLOW ITERATIVE SCHEME

The time-stepping version of the code includes a viscous/potential flow iteration loop which is used to establish the extent of tip-edge separation. The calculation is performed in the steady mode at the mean angle of attack, the results of which can be used to set the extent of tip-edge vortex separation for the unsteady calculation.

The rectangular tip was used to test the procedure for calculating the location of the tip-edge separation and boundary layer calculations. Presented here is a sample case.

Following a steady calculation at the mean angle of attack, a family of surface streamlines were calculated, Figure 8. Boundary layer layer calculations were then performed along each streamline. The boundary layer code is an integral method based on locally axisymmetric conditions with the surface curvature and streamline convergence/divergence effects included. First, calculations were performed in the steady mode to establish the extent and location of separation lines as a function of angle of attack. Angles of 4^{o}, 8^{o}, 12^{o} and 16^{o} were analyzed. In each case a family of streamlines was calculated. Figure 9 shows the extent of separation as a function of angle of attack and two Reynolds numbers. The lines represent the conditions for the first iteration; i.e., before modeling the edge vortex. The low Reynolds number corresponds with the unsteady experiment while the higher Reynolds number is more representative of full-scale conditions.

Figure 10 shows the plan view of the calculated separation boundaries for a range of angles of attack. In addition to the tip-edge separation, the separation boundaries over the inner part of the wing are also included. Figure 10(a) shows the boundaries for the model Reynolds number of 1.28×10^{6} and Figure 10(b) is for a full-scale Reynolds number of 6.0×10^{6}. At the lower Reynolds number, some laminar separation with no reattachment is indicated at 18^{o} in the inboard region. At the higher Reynolds number, the extent of separation is considerably lower and would probably have some impact on dynamic stall qualities relative to the model data. For the purposes of the model scale Reynolds number, the inboard separation appears to be small enough to be neglected for angles of attack up to 12^{o}.

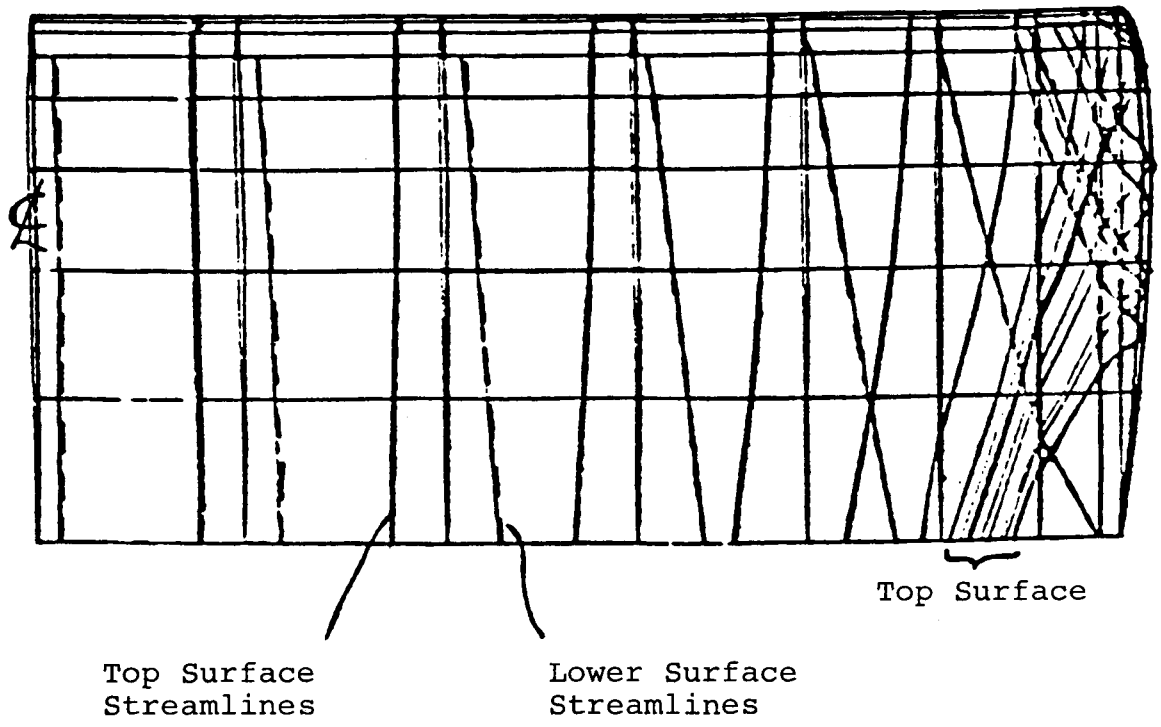

Figure 8. Calculated Streamlines on Rectangular Tip.

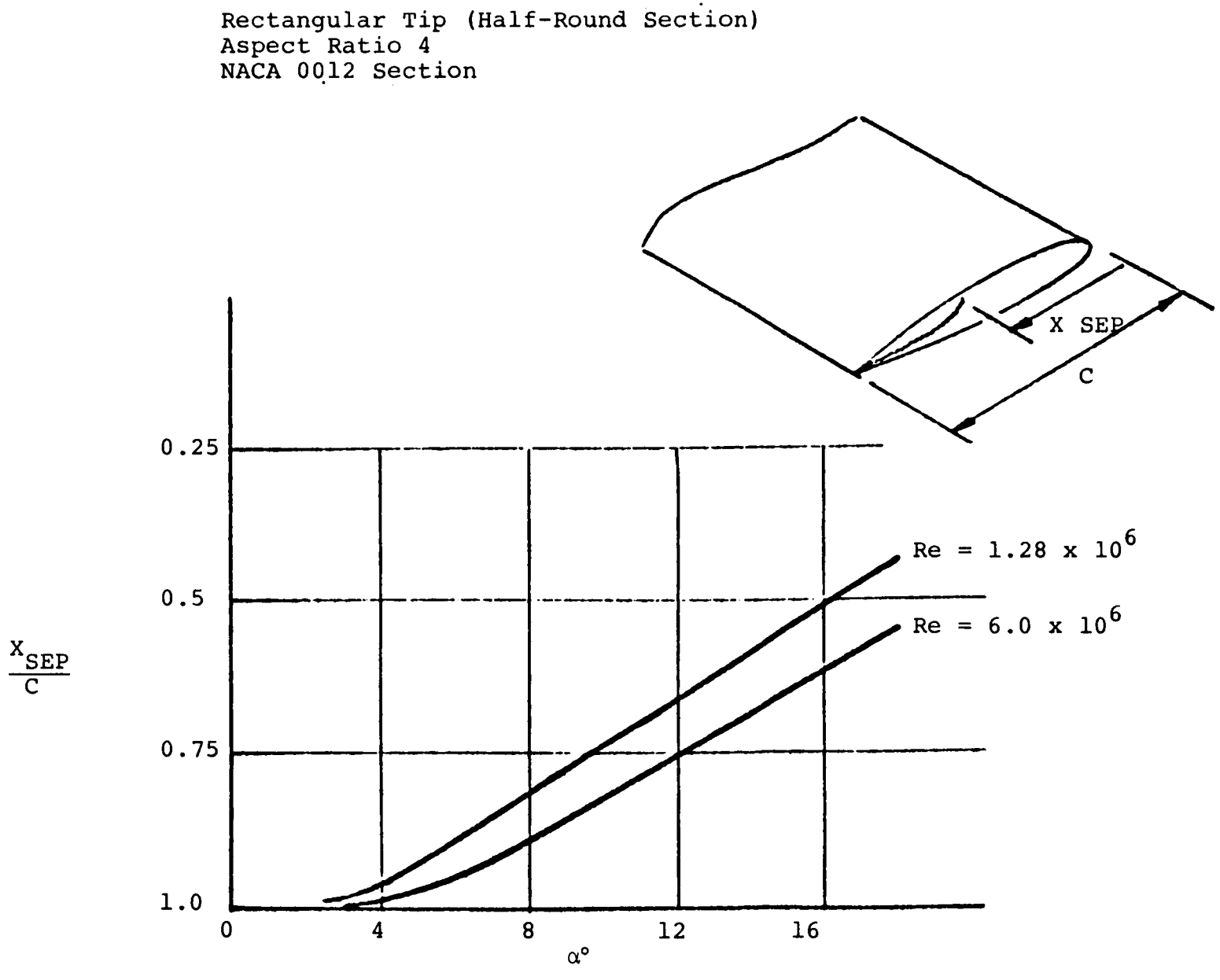

Figure 9. Effect of Angle of Attack on Extent of Tip-Edge Separation.

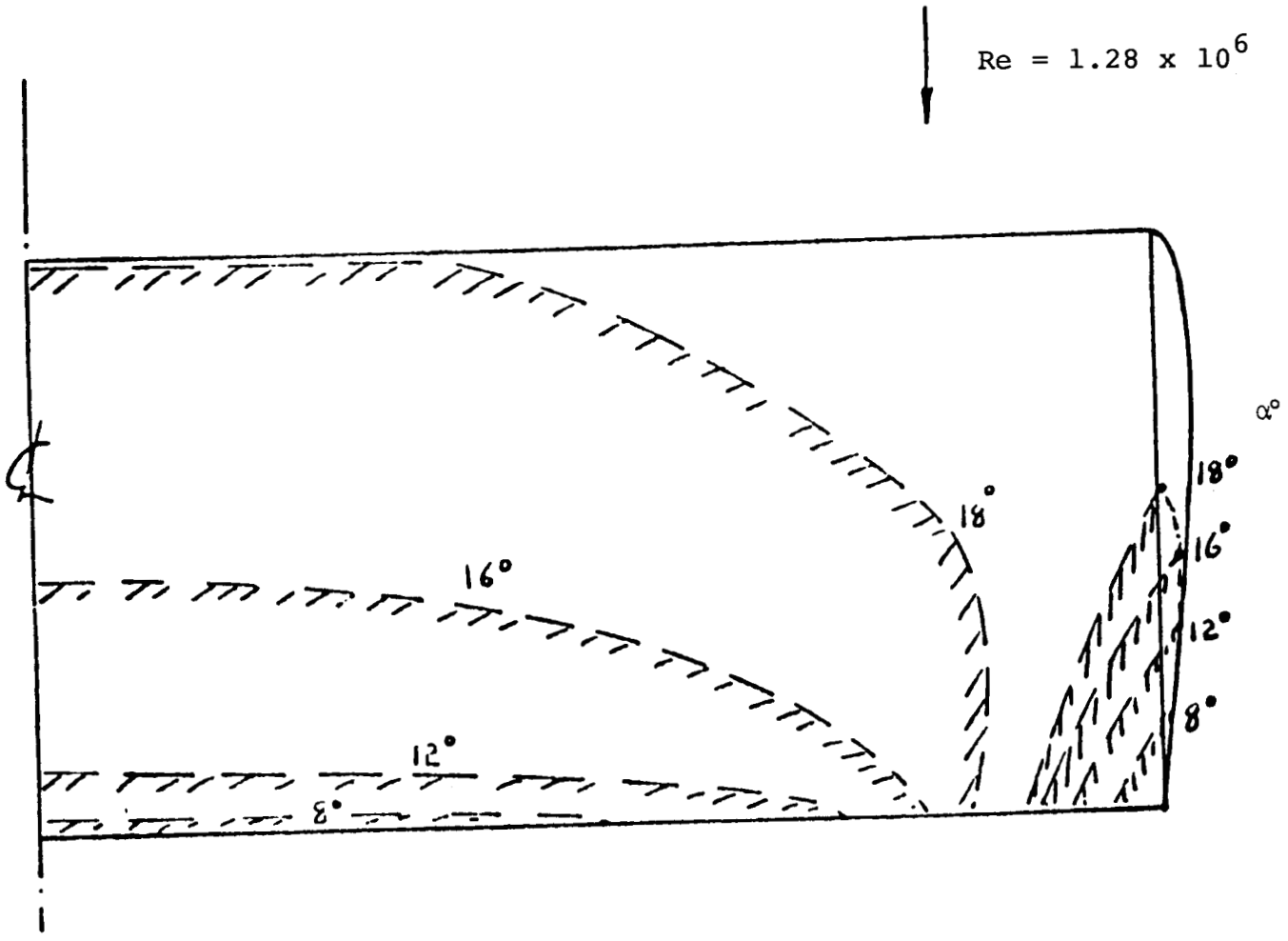

(a) Reynolds Number 1.28 x 10^6.

Figure 10. Calculated Separation Boundaries for a Range of α.

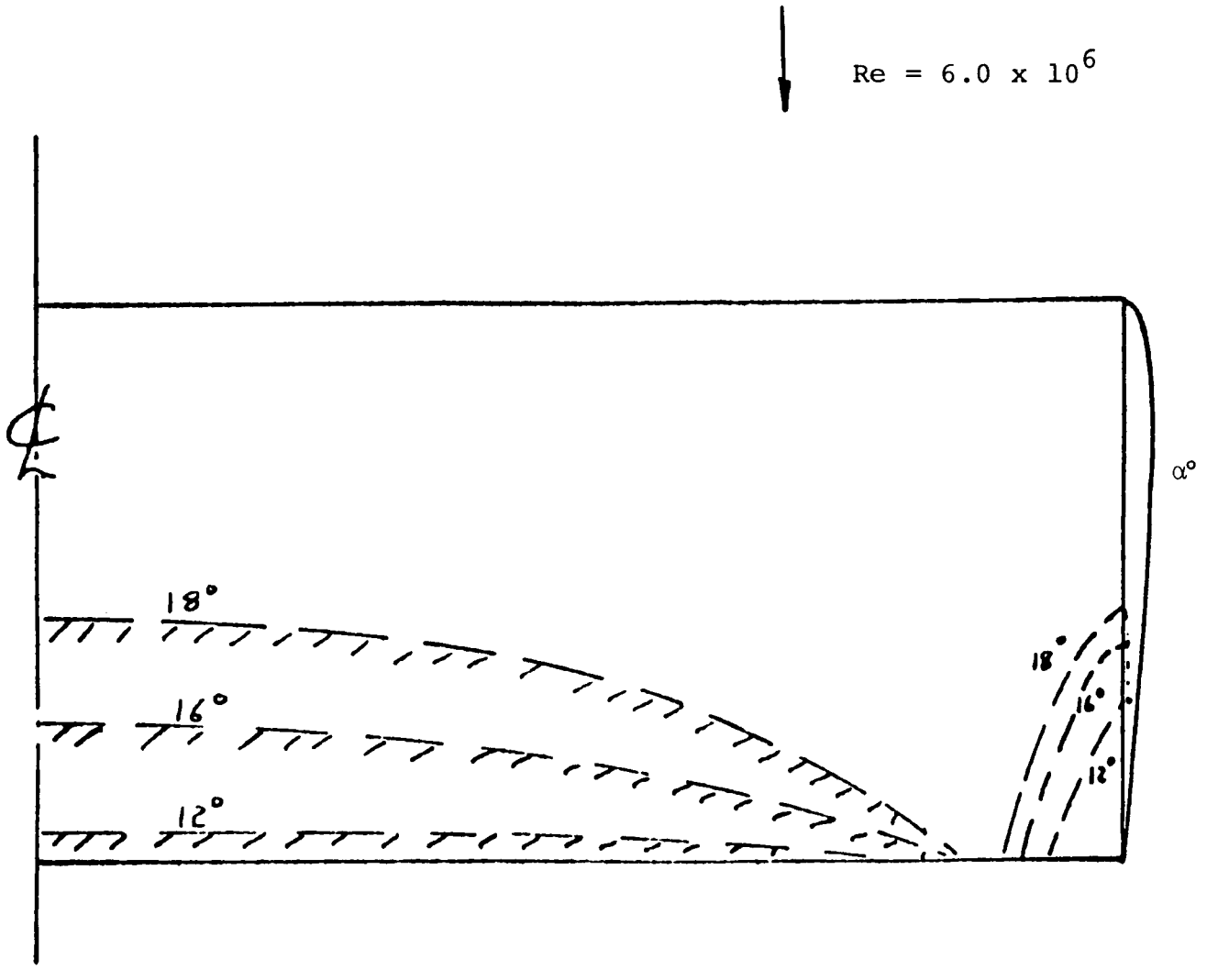

(b) Reynolds Number 6.0 x 10^6.

Figure 10. Concluded.

6.0 'VSAERO-H': DISCUSSION ON WAKE INTEGRAL AND CONVERGENCE CHARACTERISTICS

Program VSAERO-H uses harmonic wake and small amplitude assumptions. The governing flow equation is

$$\sum_{\substack{K=1 \\ K\neq J}}^{N_S} (\mu_K C_{JK}) - 2\pi\mu_J + \sum_{K=1}^{N_W} (\mu_{WK} C_{JK}) + \sum_{K=1}^{N_S} (\sigma_K B_{JK}) = 0; \qquad J=1, N_S \tag{8}$$

where N_S and N_W are the number of surface and wake panels.

In the case of harmonic flow, the application of the unsteady Kutta condition enables one to express the doublet strength in a wake strip in terms of its strength at the beginning of the strip. The wake contribution in Eq. (8) is replaced by

$$\sum_{K=1}^{N_{Ws}} \mu_{WK_o} C_{JK},$$

where μ_{Ws} is the number of spanwise (wake) strips and μ_{WK_o} is the doublet strength at the beginning of the k^{th} wake strip, and

$$C_{JK} = \iint_{\text{Wake Strip K}} e^{-i\omega(x-x_s)n} \cdot \nabla \frac{1}{r_J} \, dS.$$

The convergence characteristics of the wake integral were thoroughly investigated by adopting the following mathematical model. The wake influence coefficients (ϕ) are computed using an analytic expression for spanwise integration and a numerical scheme for chordwise integration from the trailing edge to infinity. However, due to the highly convergent nature of the ϕ integrand, which is inversely proportional to r^3, it is only necessary to integrate a few chord lengths behind the trailing edge. A series of convergence studies are conducted to evaluate the computational efficiency of the wake influence coefficients. Two singularity models, a constant doublet distribution and a linear doublet distribution over each wake panel were evaluated.

Figure 11 shows the model used for the numerical scheme in the present study. The doublet distribution in the wake is assumed to be

$$\mu_o (1 - y/b)^2 e^{-i\omega x}$$

where μ_o is the doublet strength at the mid-span trailing edge of the wing, b is the semi-span, and ω is the reduced frequency. The wake integrals are evaluated by summing the contributions of several spanwise strips covering the entire wing span. For chordwise integration, two doublet models, a constant distribution and a linear distribution are used. For the constant doublet distribution model, the doublet strength at any spanwise strip,

$$\mu_t e^{-i\omega x}$$

is assumed to be a constant and is equal to the strength at the center of the chosen wake strip. For example, the doublet strength at the n^{th} wake strip is assumed to be

$$\mu_t e^{-i\omega x_n}$$

where x_n is the center of the n wake strip, and the contribution is computed numerically over the strip width, Δx_n. For the linear doublet distribution model, a wake strip influence is computed by summing the contribution of the two terms, the doublet strength at the leading edge of the strip,

$$\mu_t e^{-i\omega (x_n - x_n/2)}$$

and the incremental doublet strength,

$$\mu_t \left[e^{-i\omega x_n} - e^{-i\omega (x_n - \Delta x_n/2)} \right]$$

Figure 12 shows the convergence characteristics of the wake influence coefficients as the panel size in the wake varied from 1/4 to 4 widths of the trailing-edge panel. As can be seen from Figure 11, the linear doublet distribution model improves the convergence characteristics and hence this model is used in the program.

Additionally the numerical results for ϕ were compared with those of analytical results presented in Reference 10. The wake model used for this computation is presented in Figure 13 and the comparison of the results for both wake models, constant and linear doublet, are presented in Table I. As can be seen, the comparison is excellent, validating the numerical scheme adopted in the current program.

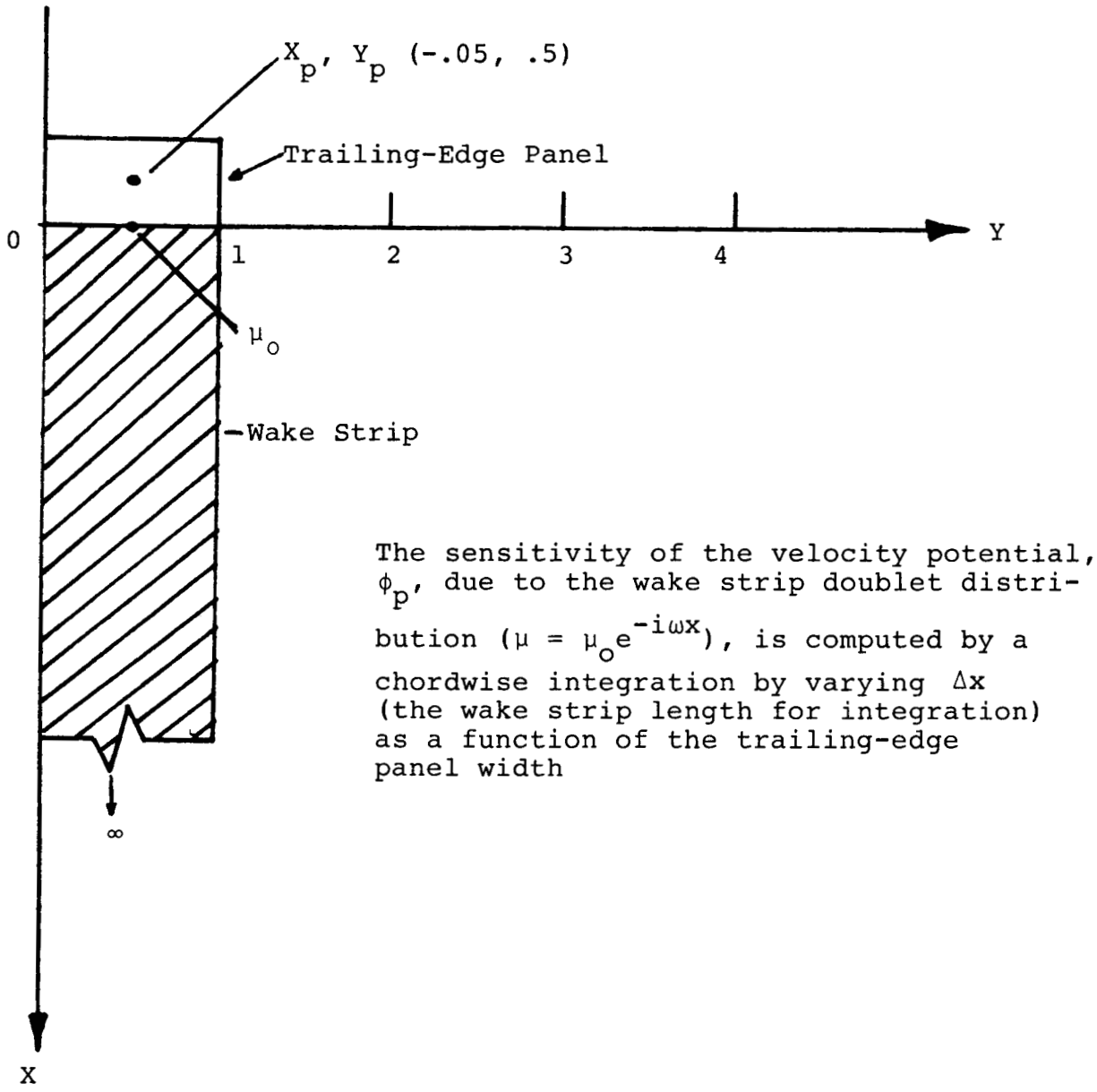

Figure 11. Model used for Convergence Study.

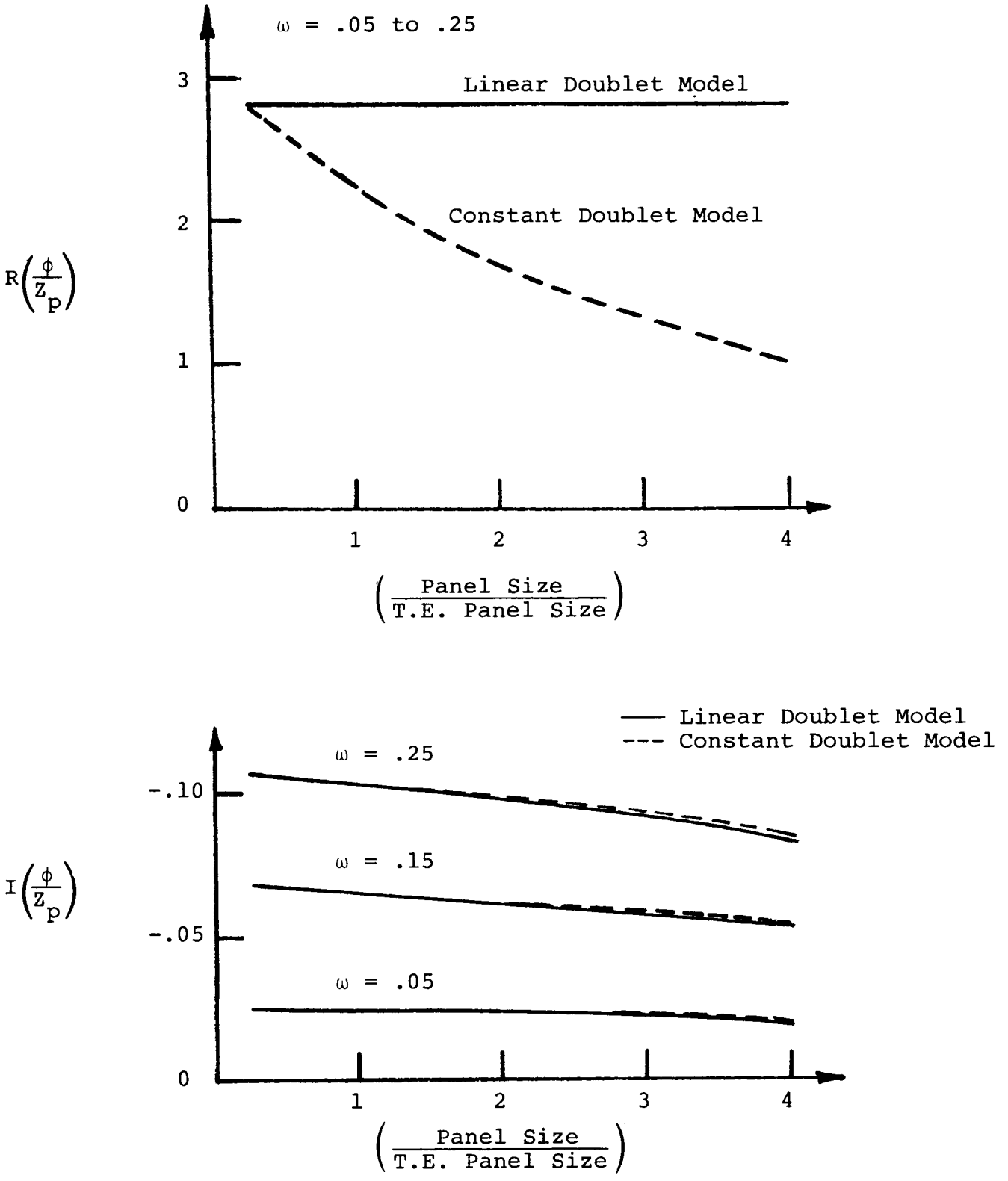

Figure 12. Influence Coefficient Versus Panel Size for Two Wake Doublet Models.

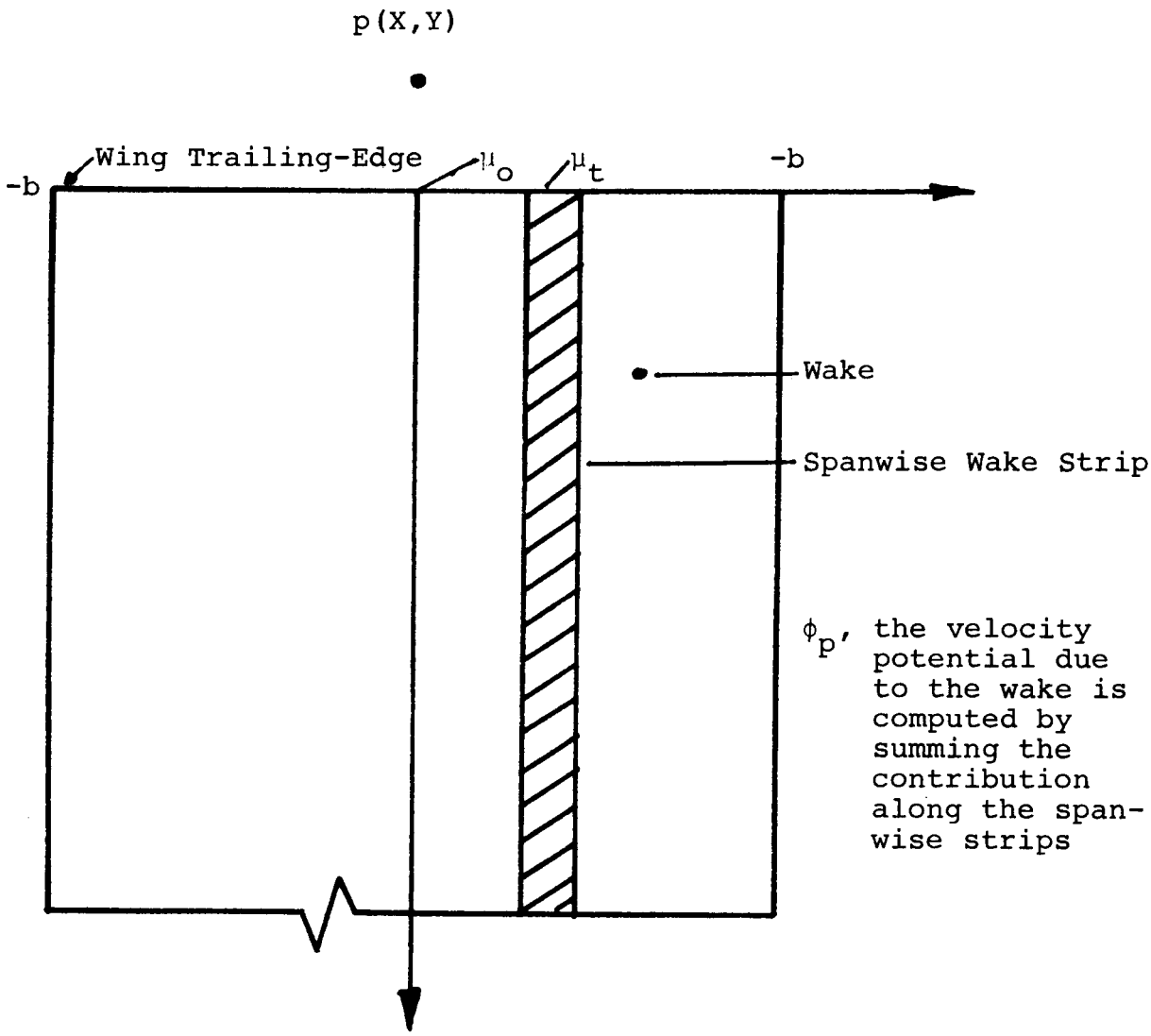

Figure 13. Model used for Wake Integral Computations.

CONSTANT DOUBLET MODEL; $\Phi_p \times 10^3$, Y = .1, Z = .1.

ω	x	ANALYTICAL (Send)	COMPUTED		
			Δx = .025	Δx = .1	Δx = .4
.1	-1.5	1.233 - .286i	1.236 - .286i	1.235 - .286i	1.214 - .288i
.1	-1.0	2.810 - .472i	2.827 - .473i	2.822 - .473i	2.727 - .480i
.1	-.5	10.300 - 1.012i	10.502 - 1.022i	10.428 - 1.026i	9.454 - 1.057i
.5	-1.5	.700 - .551i	.700 - .554i	.699 - .555i	.678 - .566i
.5	-1.0	1.915 - 1.140i	1.927 - 1.114i	1.921 - 1.115i	1.825 - 1.179i
.5	-.5	8.510 - 3.221i	8.701 - 3.257i	8.627 - 3.271i	7.644 - 3.426i

LINEAR DOUBLET MODEL; $\Phi_p \times 10^3$, Y = .1, Z = .1.

ω	x	ANALYTICAL (Send)	COMPUTED		
			Δx = .025	Δx = .1	Δx = .4
.1	-1.5	1.233 - .286i	1.237 - .286i	1.237 - .286i	1.236 - .289i
.1	-1.0	2.810 - .472i	2.827 - .473i	2.827 - .474i	2.827 - .484i
.1	-.5	10.300 - 1.012i	10.507 - 1.010i	10.507 - 1.028i	10.505 - 1.073i
.1	-1.5	.700 - .551i	.700 - .554i	.700 - .555i	.697 - .571i
.1	-1.0	1.915 - 1.140i	1.923 - 1.144i	1.927 - 1.149i	1.918 - 1.194i
.1	-.5	8.510 - 3.221i	8.706 - 3.257i	8.703 - 3.282i	8.667 - 3.498i

Table 1. Comparison of Computed and Analytical Unsteady Velocity Potential (Φ_p).

7.0 RESULTS AND DISCUSSION ON CONVERGENCE CHARACTERISTICS

In this section a limited number of results are presented for the four tip planforms to demonstrate the convergence characteristics of VSAERO-TS as a function of reduced frequency and the number of time steps per cycle. A complete set of the results may be found in Reference 1 in comparison with experimental data.

7.1 Rectangular Tip--Parametric Studies

An extensive set of calculations have been performed using VSAERO-TS. Basically, calculations were performed using 60 to 120 time steps over 3 half cycles.

(1) Effect of Panel Density

First, the effect of panel density was examined:

(a) 30 (chordwise) x 4 (spanwise) plus 3 (vertical) x 15 (chordwise) on the tip

(b) 40 x 4 + 3 x 20

(c) 30 x 8 + 3 x 15

The calculations were performed for ω = 0.3 (based on half-chord), α_i = 1° and α_o = 12°. The wake length was 10 chords with 25 wake panels down each strip and N = 120 (time steps). The effect of chordwise panel density is given in the table below which compares the unsteady lift and moment coefficients at two spanwise stations.

Spanwise Station y/s		Panels 30 x 4 + 3 x 15	Panels 40 x 4 + 3 x 20
0.25	C_L	4.42 + 1.17i	4.42 + 1.17i
	C_M	0.573 - 0.517i	0.563 - 0.513i
0.95	C_L	2.52 + 0.86i	2.52 + 0.86i
	C_M	0.098 - 0.395i	0.079 - 0395i

Table 2. Effect of Chordwise Panel Density on Spanwise Lift and Moment Distributions.

The results are therefore essentially converged with 30 chordwise panels. In fact, they are converged even for as few as 20 chordwise panels. The chordwise distribution of panels is the default form, which increases panel density towards the leading edge.

The effect of spanwise panel density is shown in Figure 14 for the unsteady lift distribution. Four spanwise intervals clearly give a very good account; however, for details of the behavior near the tip the eight spanwise intervals case probably represents a minimum density. Both distributions used a "cosine" spacing with density increasing towards the tip.

(2) Effect of Wake Length

The effect of wake length (i.e., the length of wake represented by the wake doublet panels) was examined. Presented below are the integrated unsteady lift and moment characteristics at the inboard and outboard stations, for the case of α_o = 12°, α_i = 1°, and ω = 0.30.

Spanwise Station y/s		Wake Length: 10 Chords	Wake Length: 20 Chords
0.25	C_L	4.48 + 1.24i	4.47 + 1.25i
	C_M	0.038 - 0.441i	0.042 - 0.439i
0.95	C_L	2.27 + 0.88i	2.27 + 0.88i
	C_M	-0.011 - 0.280i	-0.011 - 0.280i

Table 3. Effect of Wake Length on Spanwise Lift and Moment Distributions.

The results are essentially converged with a wake length of 10 chords. Although not presented in this document, the wake length of 10 chords proved to be adequate even for the case of low reduced frequency of 0.1.

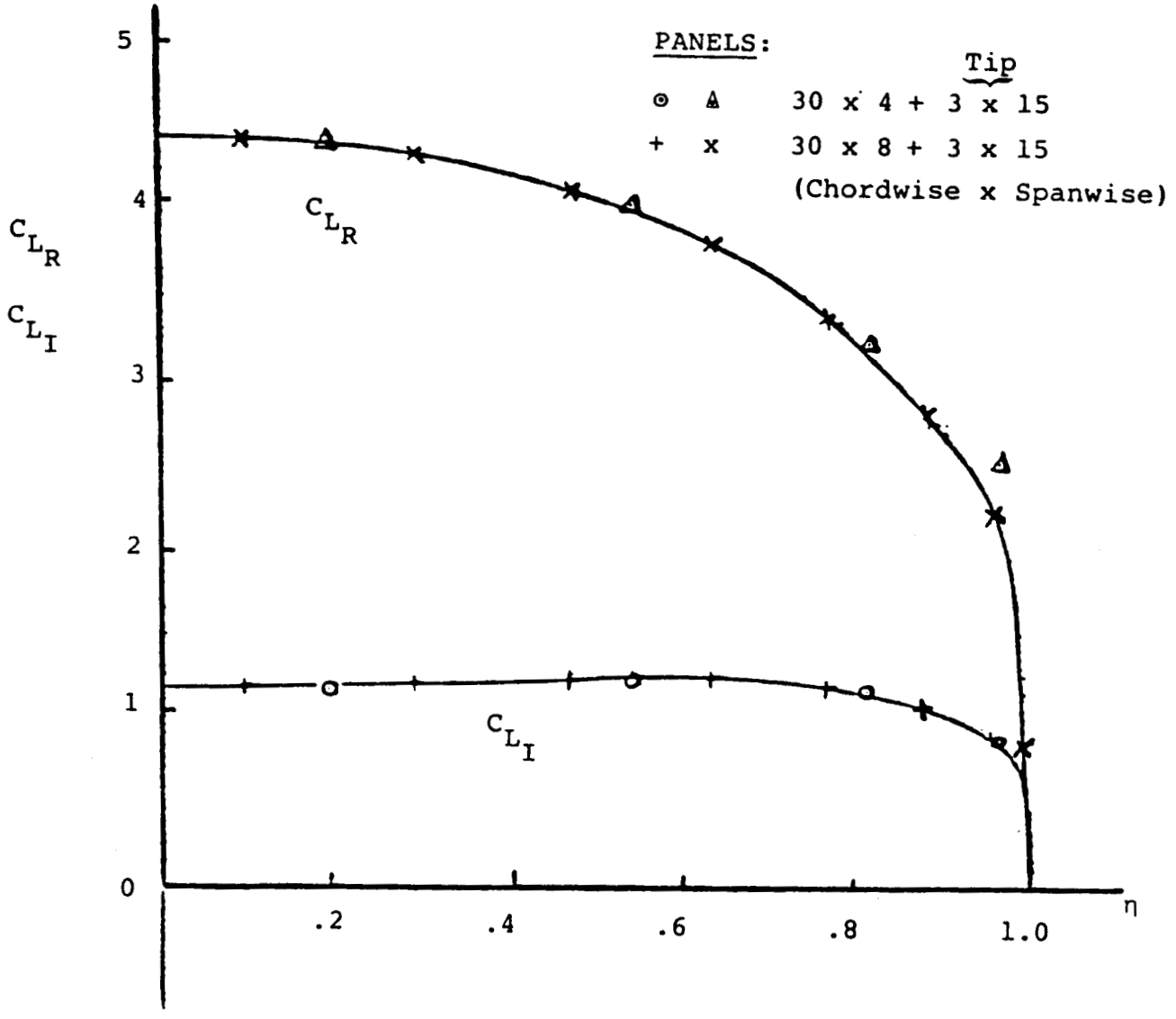

Figure 14. Calculated Unsteady Lift Distribution--Effect of Spanwise Panel Density (α_o = 12°, α_i = 1°, ω = 0.30).

(3) Effect of Number of Time Steps

For the case of α_o = 12°, α_i = 1°, ω = 0.30, and wake length of 10 chords, the number of time steps was varied between 40 and 120. Table 4 compares the integrated unsteady lift and moment coefficients at several spanwise stations.

This example demonstrates that N = 60 is adequate to obtain convergent results. However, for the low reduced frequencies, N = 120 is required for the proper convergence.

Additionally, some typical results for the rectangular tip are presented in Figures 15 and 16 for reduced frequencies of 0.1 and 0.3, respectively. The chordwise pressure distributions at two spanwise stations (y/s and 0.25 and 0.95) are compared with those of the DFVLR test results. Figures 15(a) and (b) show the chordwise distributions at the two spanwise stations for ω = 0.1; the computed results for these are obtained using the standard VSAERO-TS quadrilateral panels. For the present case of high angle of attack, this approach is inadequate to handle the roll-up of the tip vortex due to the problem of panel skew. Hence, the modified VSAERO-TS, in which the quadrilateral panels in the wake are temporarily replaced by pairs of triangular panels, is used and the results are shown in Figures 15(c). As can be seen the comparison between the computed and test results has substantially improved. Figures 15(d) and (e) show the instantaneous tip vortex wake geometry for this particular case. Figures 16(a) and (b) show the chordwise pressure distributions for ω = 0.3 at the root and tip sections. In general, the comparison is good for both real and imaginary parts.

7.2 Swept Tip

This particular case is used to investigate the effect of wake transport length for each time step. In order to maintain the same level of wake detail, the number of time steps for each cycle in VSAERO-TS must be inversely proportional to the reduced frequency. The swept tip case is considered and the number of time steps are varied between 120 and 40 as reduced frequency is varied between 0.1 and 0.3.

Figures 17(a), (b) and (c) show the comparison of the chordwise pressure distribution between VSAERO-TS and the DFVLR test results at a 60% spanwise location for ω = 0.1, 0.2 and 0.3, respectively. As can be seen, the comparison is uniformly good in all these cases.

Spanwise Station Y/s		Number of Time Steps 40	60	90	120
0.25	C_L	4.50 + 1.09i	4.47 + 1.10i	4.47 + 1.13i	4.47 + 1.13i
	C_M	0.017 - 0.457i	0.026 - 0.450i	0.030 - 0.450i	0.032 - 0.450i
0.60	C_L	4.00 + 1.13i	3.98 + 1.15i	3.97 + 1.17i	3.97 + 1.18i
	C_M	0.041 - 0.443i	0.026 - 0.450i	0.053 - 0.436i	0.054 - 0.437i
0.80	C_L	3.31 + 1.10i	3.30 + 1.12i	3.29 + 1.14i	3.29 + 1.15i
	C_M	0.063 - 0.408i	0.070 - 0.404i	0.073 - 0.404i	0.074 - 0.404i
0.95	C_L	2.52 + 0.84i	2.51 + 0.86i	2.51 + 0.88i	2.51 + 0.89i
	C_M	-0.136 - 0.301i	-0.131 - 0.304i	-0.219 - 0.308i	-0.128 - 0.310i

Table 4. Effect of Number of Time Steps on Spanwise Lift and Moment Distributions.

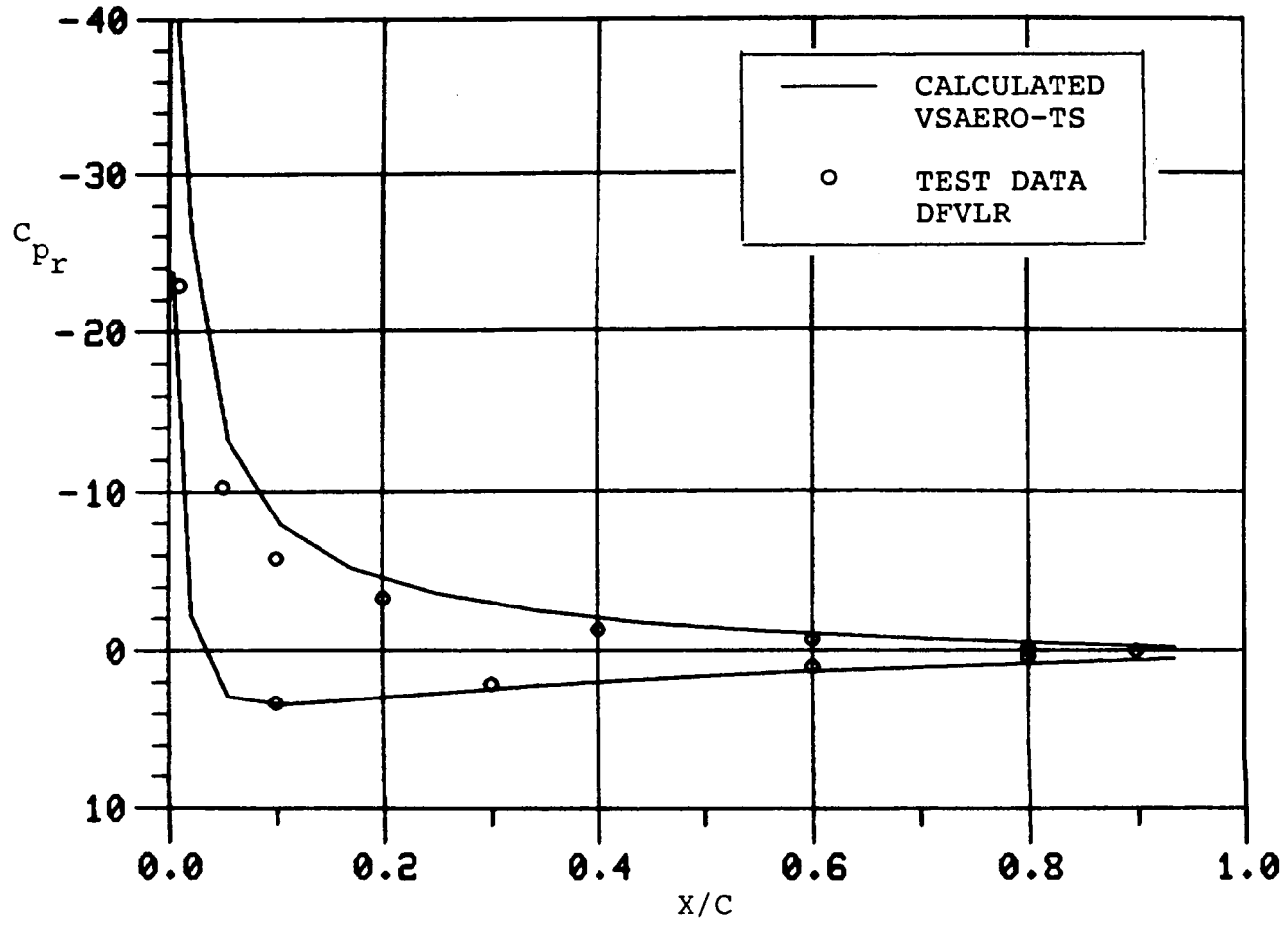

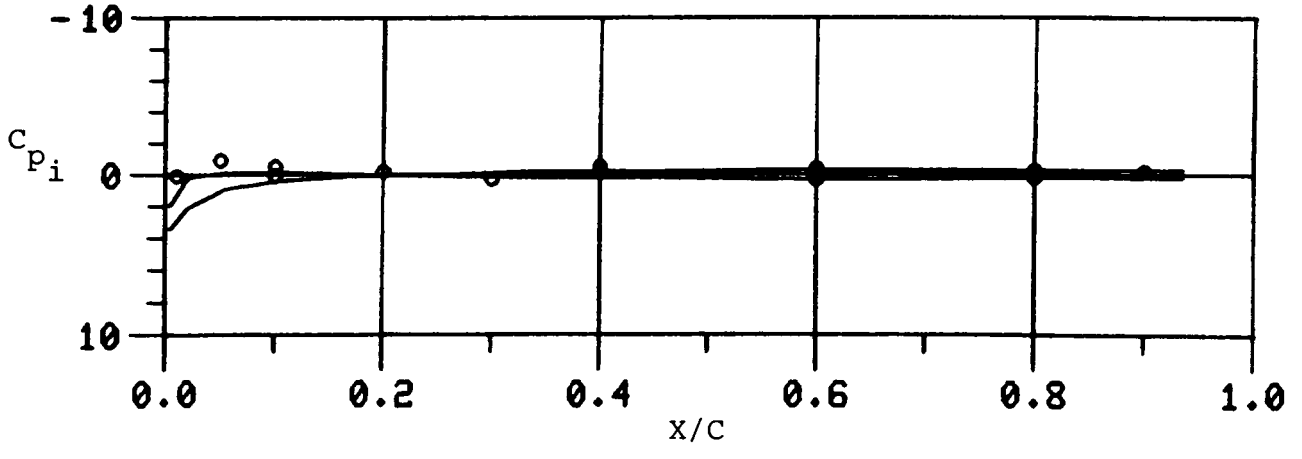

Figure 15(a). Comparison of Chordwise Pressure Distribution at y/s = 0.25 between Computed (VSAERO-TS) and DFVLR Test, Rectangular Tip (α_o = 12°, α_i = 1.066°, ω = 0.1).

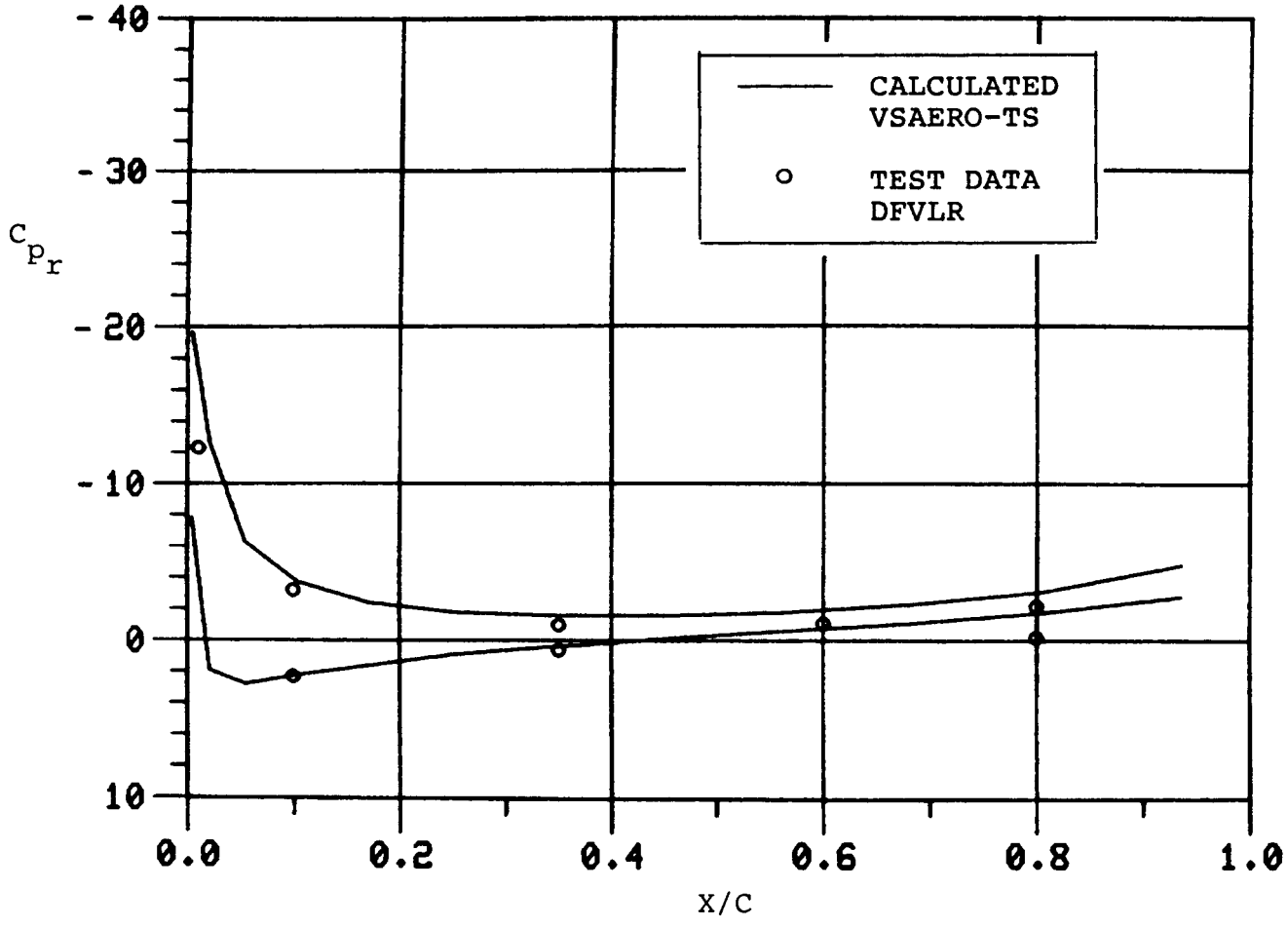

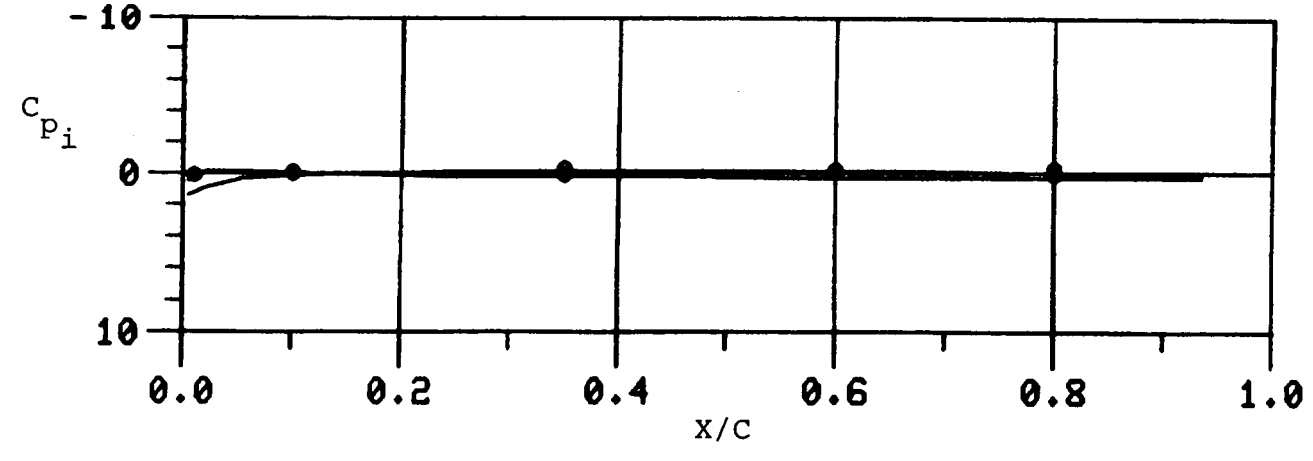

Figure 15(b). Comparison of Chordwise Pressure Distribution at y/s = 0.95 between Computed (VSAERO-TS) and DFVLR Test, Rectangular Tip (α_o = 12°, α_i = 1.066°, ω = 0.1).

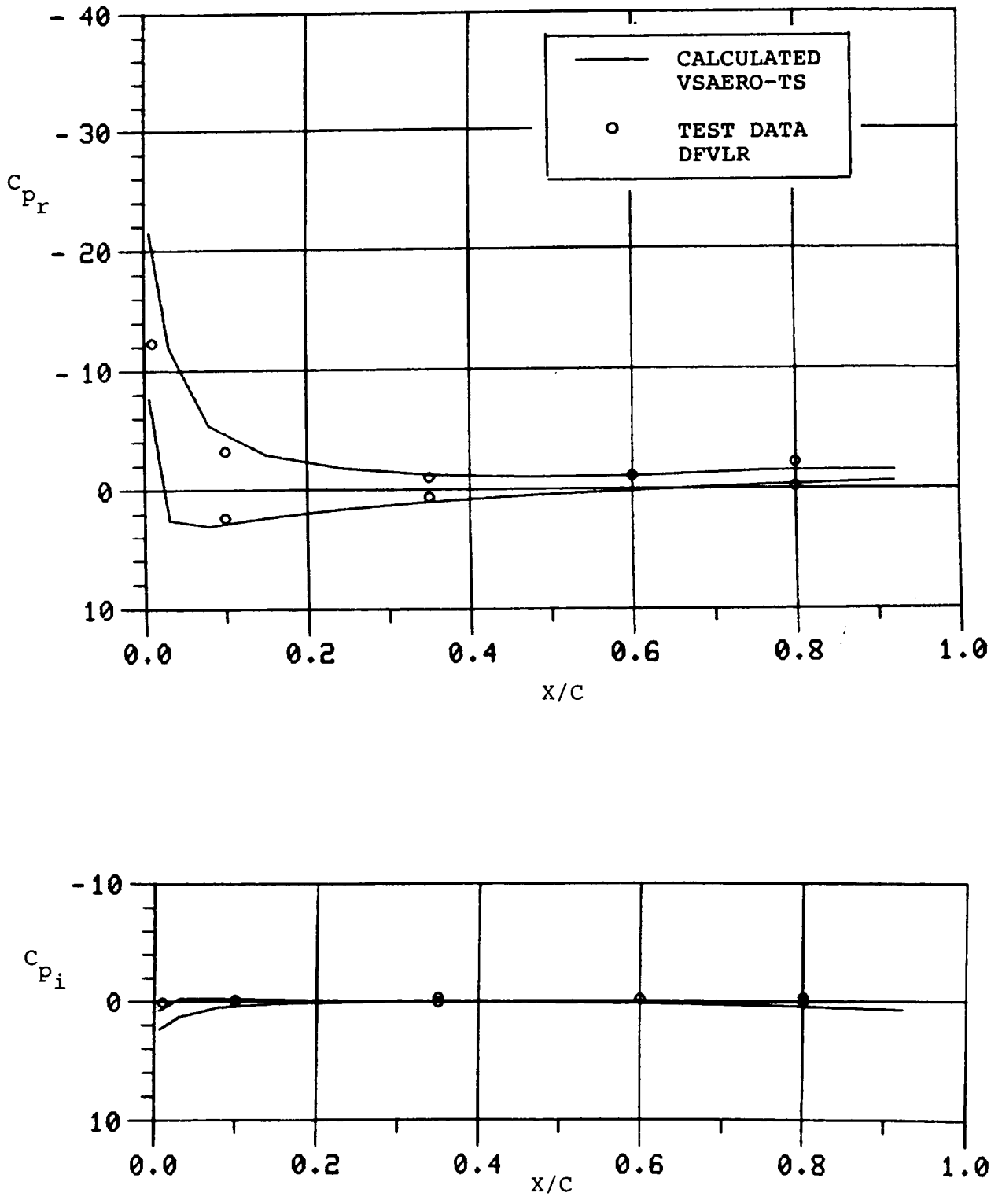

Figure 15(c). Comparison of Chordwise Pressure Distribution at y/s = 0.95 between Computed (VSAERO-TS, Triangular Panels) and DFVLR Test, Rectangular Tip (α_o = 12°, α_i = 1.066°, ω = 0.1).

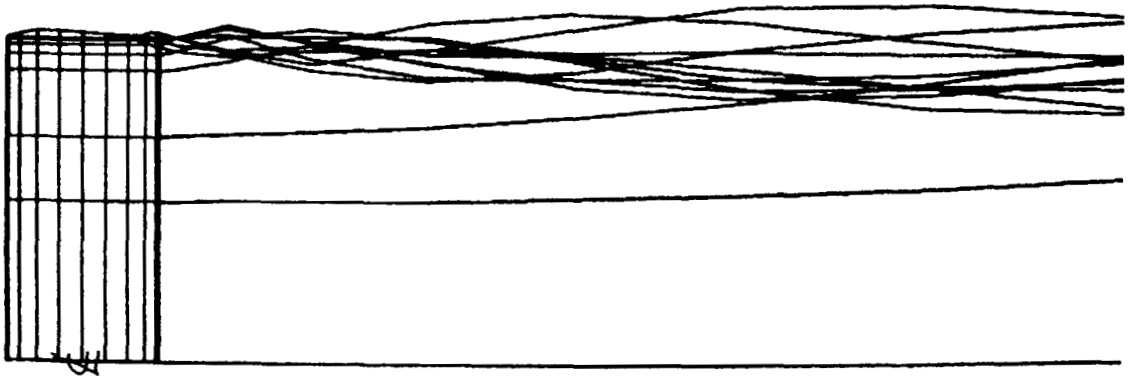

Figure 15(d). Instantaneous Wake Geometry--Plan View.

Figure 15(e). Instantaneous Wake Geometry--Side View.

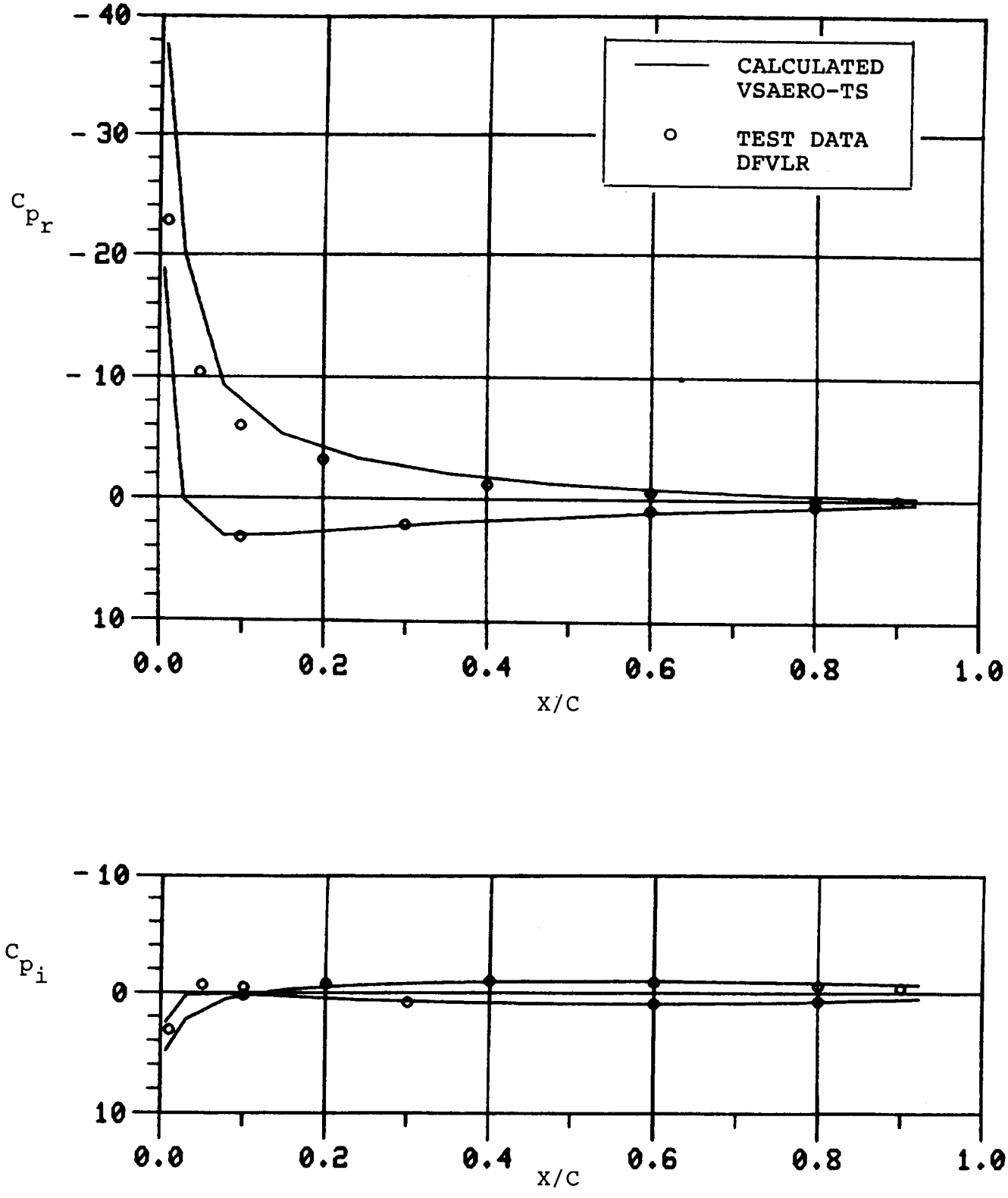

(a) At y/s = 0.25.

Figure 16. Comparison of Chordwise Pressure Distribution between Computed (VSAERO-TS) and DFVLR Test, Rectangular Tip (α_o = 12° , α_i = 1.066° , ω = 0.3).

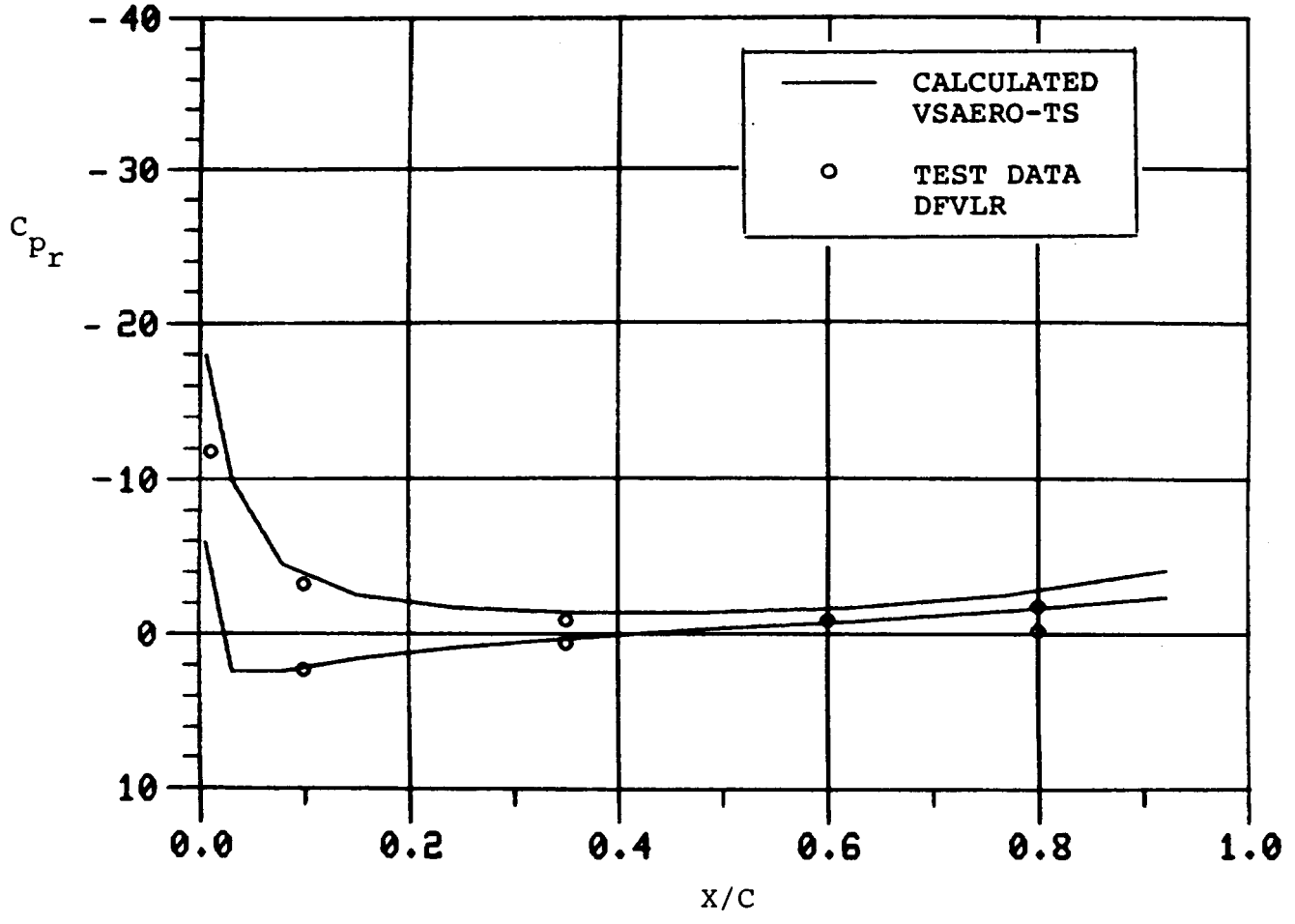

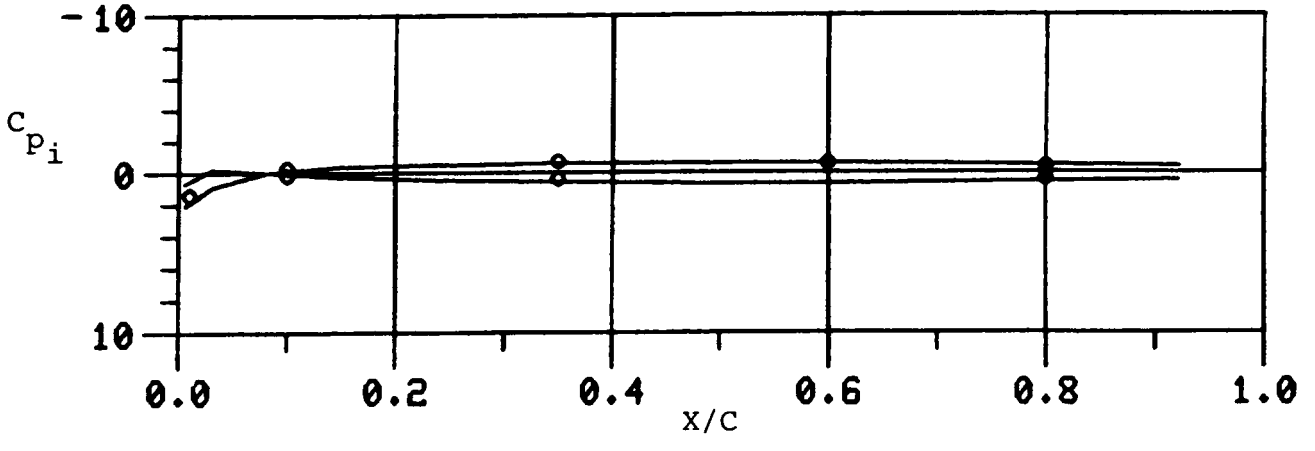

(b) At y/s = 0.95.

Figure 16. Concluded.

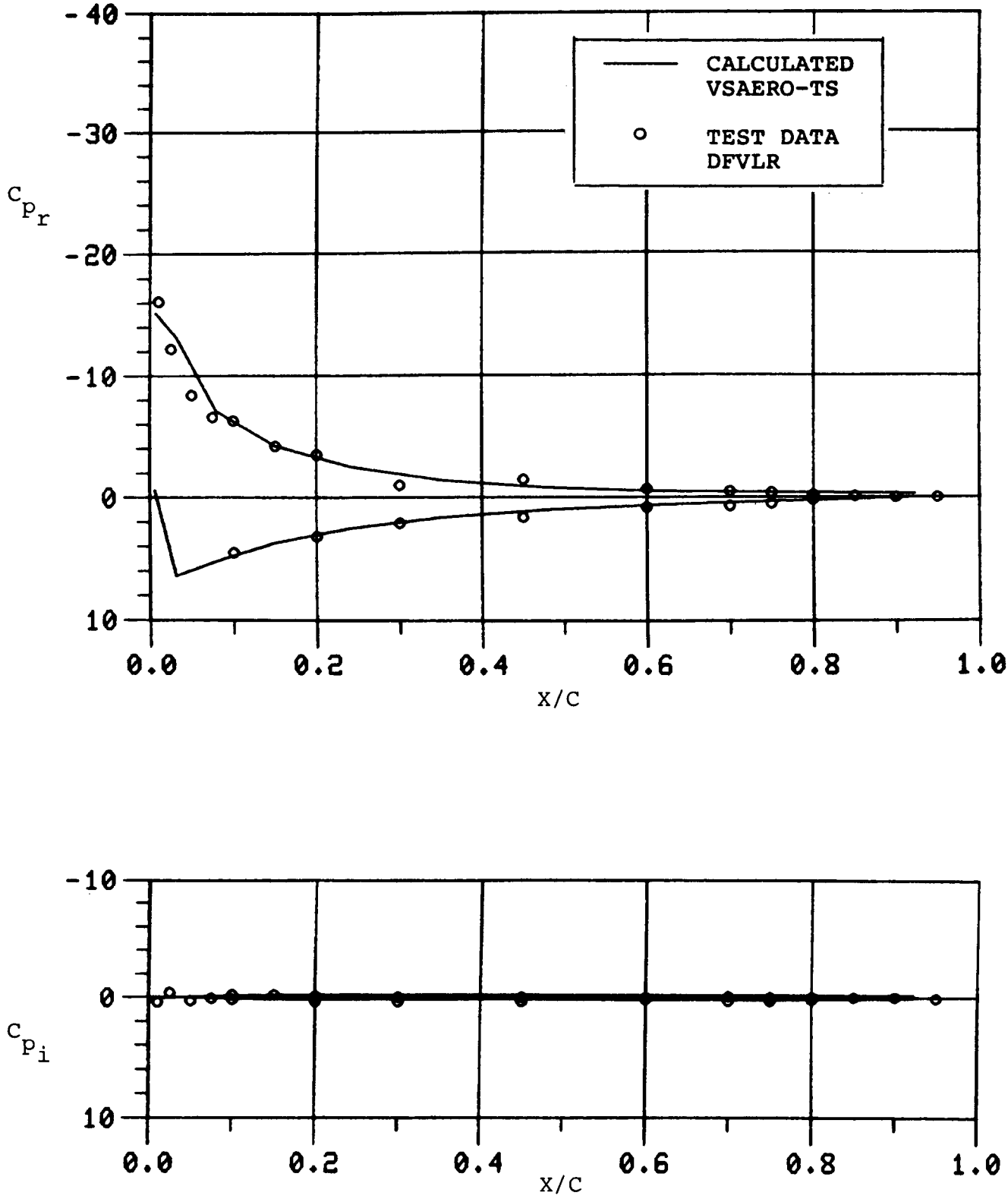

(a) At y/s = 0.60 (α_o = 4°, α_i = 0.710°, ω = 0.1, N = 120).

Figure 17. Comparison of Chordwise Pressure Distribution between Computed (VSAERO-TS) and DFVLR Test, Swept Tip.

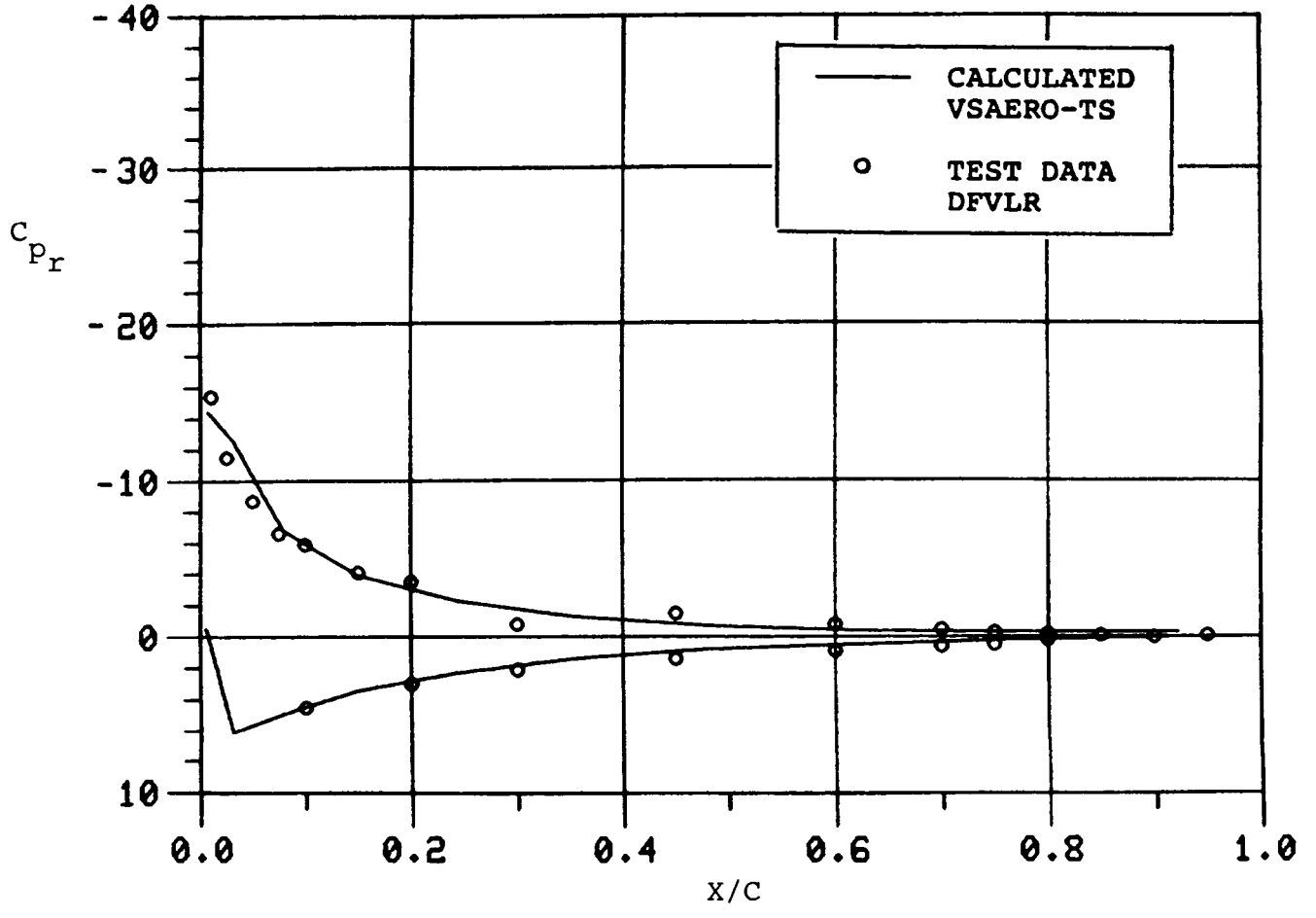

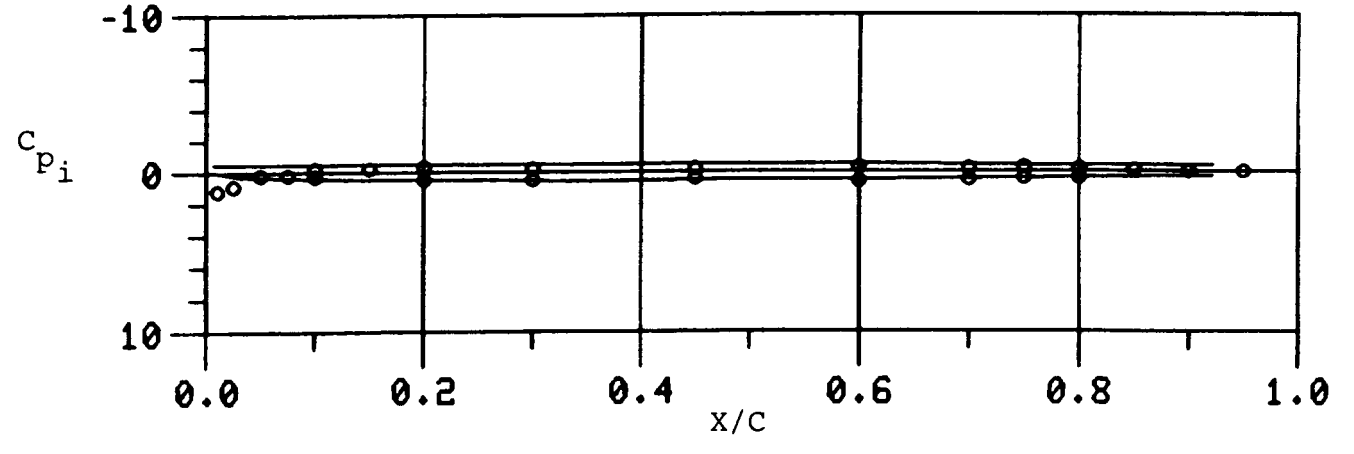

(b) At y/s = 0.60 (α_o = 4°, α_i = 0.710°, ω = 0.20, N = 80).

Figure 17. Continued.

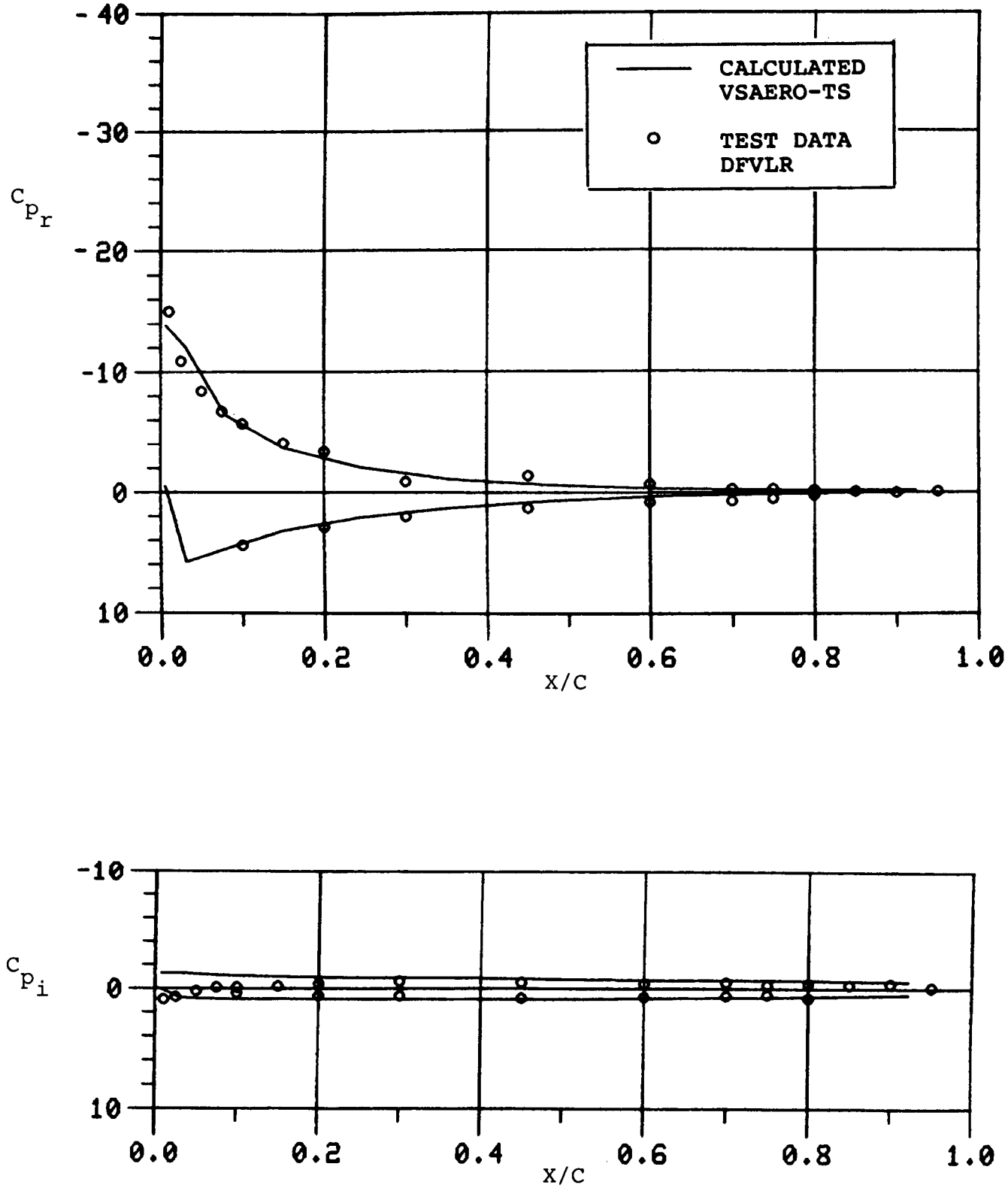

(c) At y/s = 0.60 (α_o = 4°, α_i = 0.710°, ω = 0.30, N = 40).

Figure 17. Concluded.

7.3 Ogee Tip

One case of comparison of the ogee tip chordwise pressure distribution between VSAERO-TS, VSAERO-H and the DFVLR test results is presented in Figures 18(a) and (b) for $\omega = 0.3$ at an 85% spanwise location. For this particular case the harmonic wake results appear to correlate better with the test results. However, boundary layer displacement effect is not modelled in the analysis at this time and would be expected to reduce the suction levels in both computed pressure distributions.

7.4 Spanwise Distribution of Unsteady Lift--Four Blade Tips

Figures 19(a) and (b) compare the spanwise distributions of real and imaginary lift coefficients for the four planforms for $\omega = 0.1$ and 0.3, respectively. It is emphasized that these coefficients are based on local chord. The swept and rectangular tips have almost the same distributions. The slightly larger imaginary part on the swept tip is consistent with the heaving effect caused by the rearward location of the local quarter-chord relative to the pitch axis.

A similar heaving effect is present for the tapered tip except in this case the decreasing chord lowers the effective value of the reduced frequency. Because of this, the imaginary term has taken negative values near the tip. The real part of the lift component on the tapered tip take increased values towards the tip because of the reducing chord; this is consistent with steady solutions. This effect is even more pronounced on the ogee tip; here, the increased real lift values would probably lead to separations in the outboard region. The large negative movement in the imaginary component near the ogee tip is consistent with (a) the small local chord lowering the effective value of the reduced frequency; and (b) the heaving effect caused by the local quarter-chord points located ahead of the pitch axis.

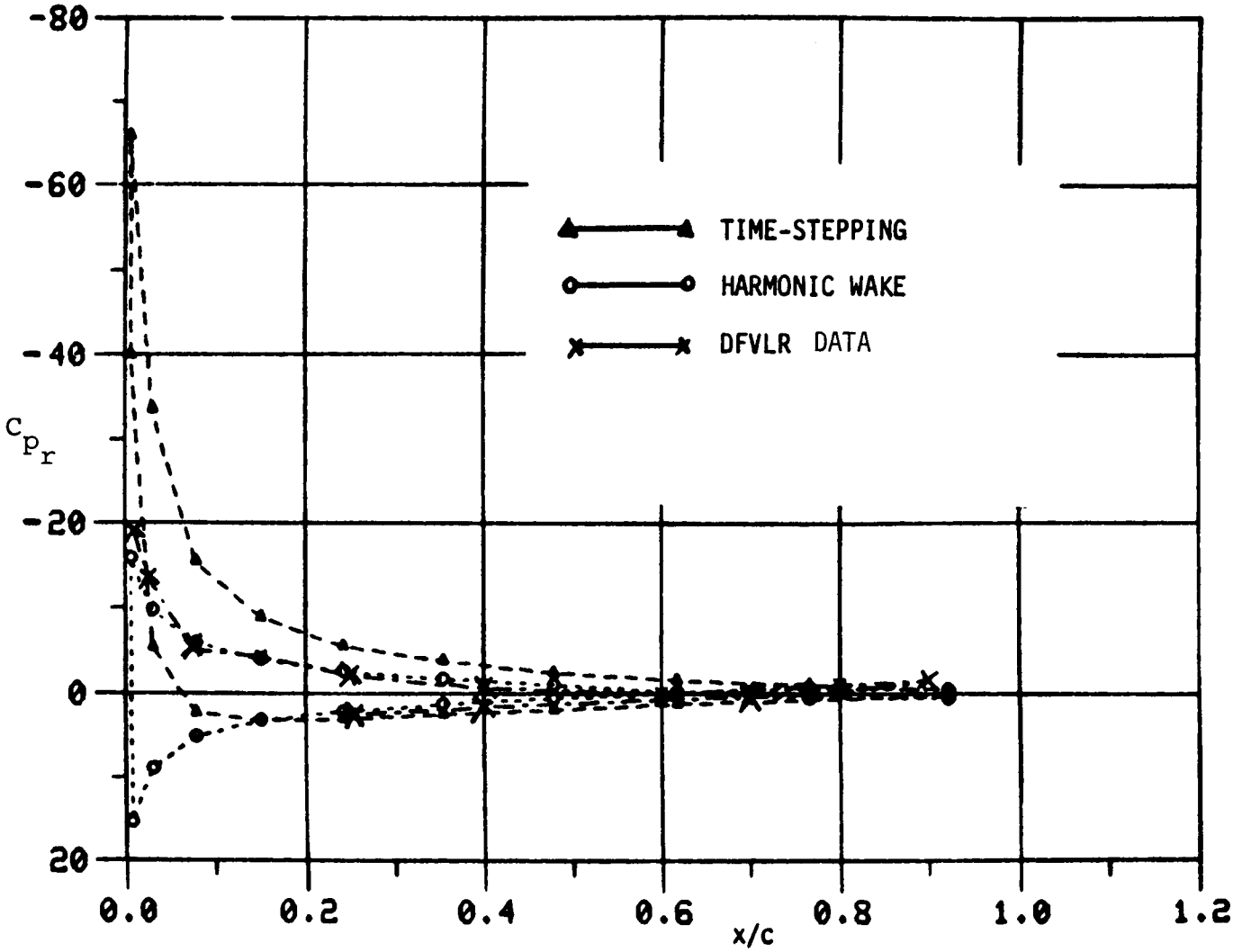

(a) Real Part.

Figure 18. Comparison of Chordwise Pressure Distribution at y/s = 0.85 between Computed and DFVLR Data; Ogee Tip (α_o = 12°, α_i = 0.710°, ω = 0.30).

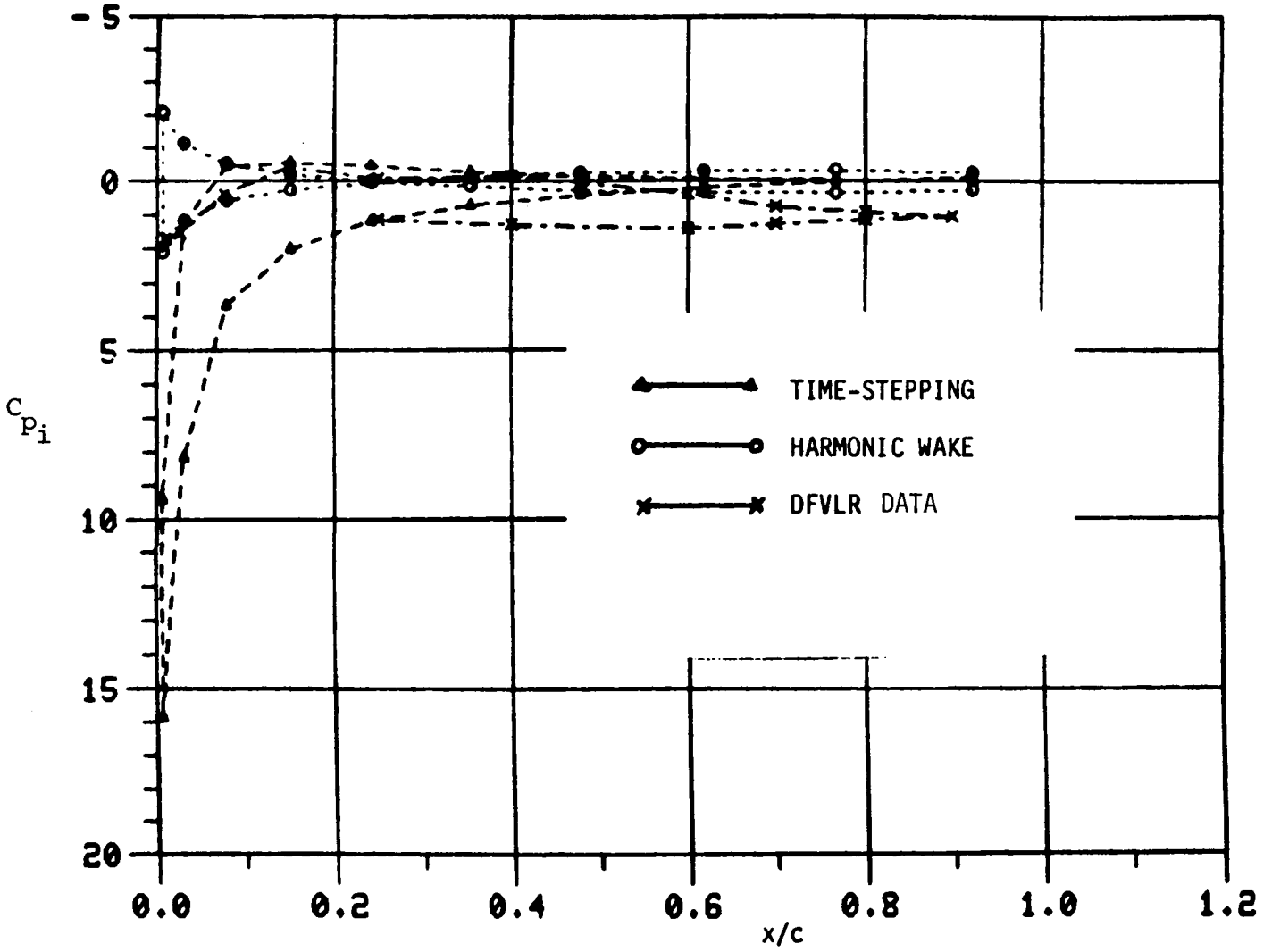

(b) Imaginary Part.

Figure 18. Concluded.

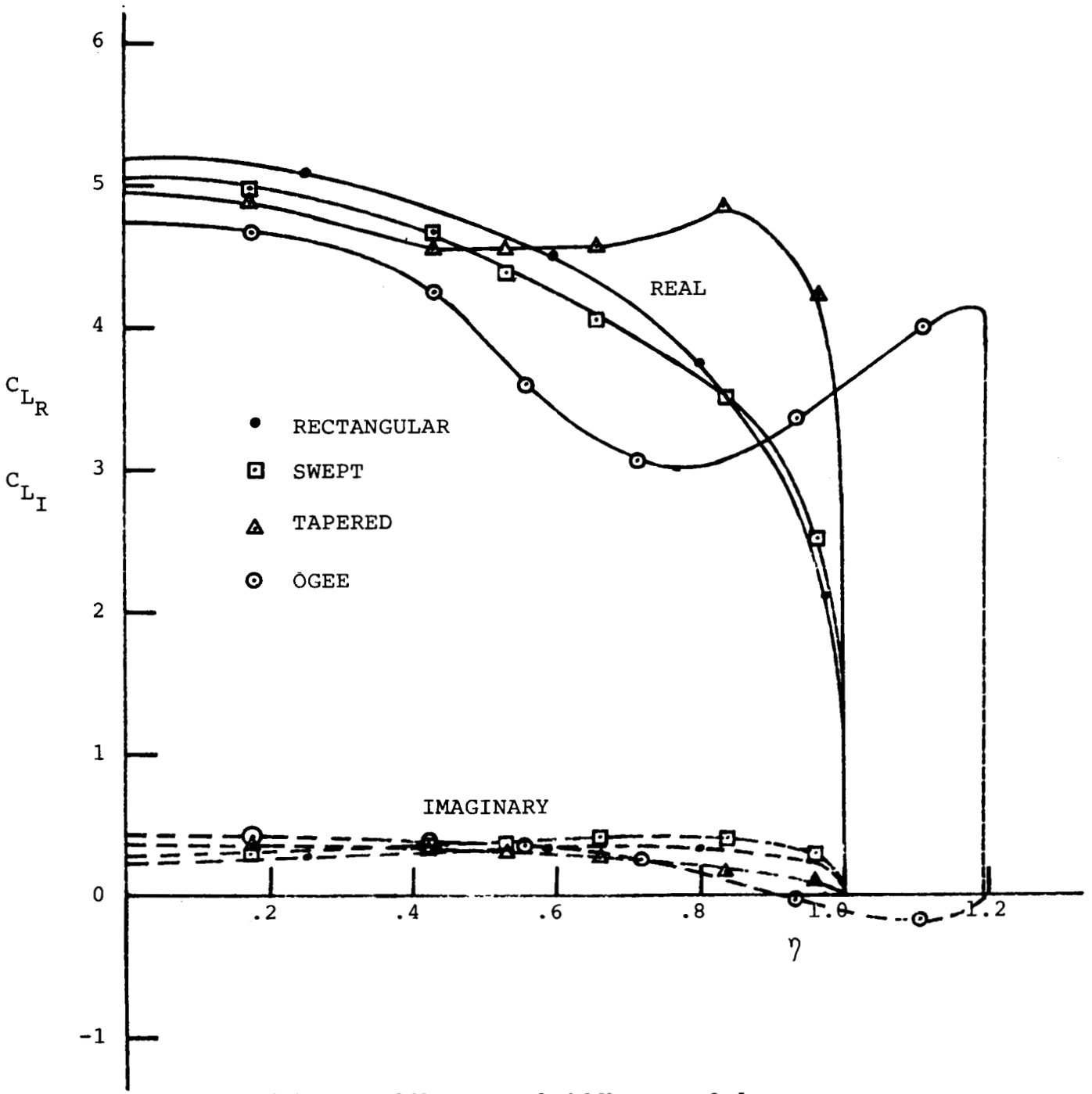

(a) $\alpha_o = 12°$, $\alpha_i = 1.066°$, $\omega = 0.1$.

Figure 19. Calculated Spanwise Distributions of Unsteady Lift for the Four Planforms (VSAERO-TS).

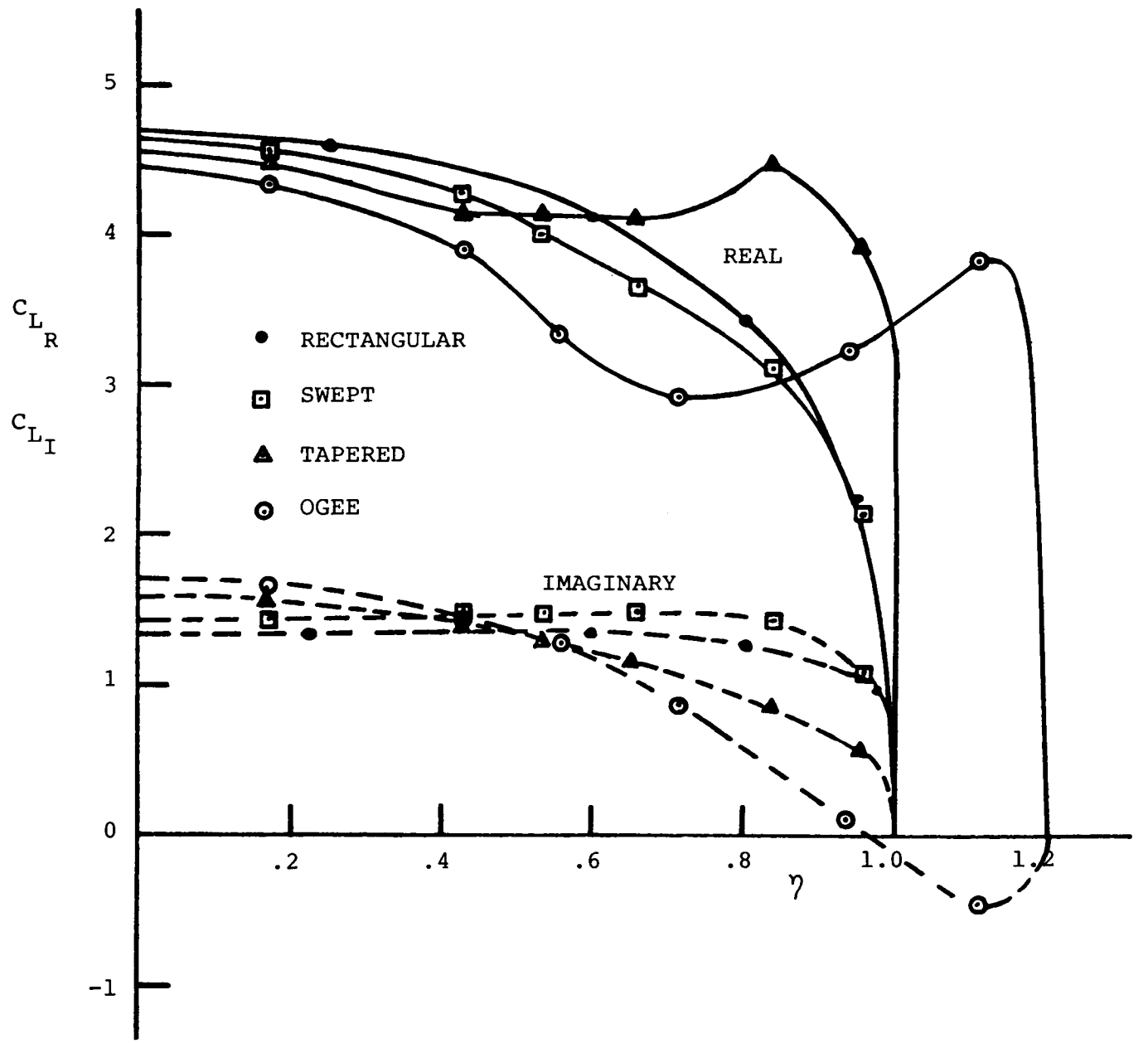

(b) $\alpha_o = 12°$, $\alpha_i = 1.066°$, $\omega = 0.3$.

Figure 19. Concluded.

8.0 SUMMARY AND CONCLUSIONS

In this report the theoretical development of two computer programs, VSAERO-TS and VSAERO-H, for calculating the unsteady aerodynamic characteristics of arbitrarily-shaped wings oscillating in pitch, is presented. The effect of several parameters--wake length, the number of time steps, and panel density--on the chordwise pressure distribution in VSAERO-TS is presented. Also, the convergence characteristics of both programs are discussed.

The treatment of the unsteady Kutta condition has been improved by a refined wake shedding model. Whereas the old model would not give consistent solutions for the ogee and tapered tip planforms, the new treatment in VSAERO-TS gives good solutions for these planforms.

In the computer programs the influence coefficient for each panel is formulated for a planar surface and so a skewed panel is represented by a projected flat quadrilateral lying in the mean plane. Panels in the extreme roll-up region of the tip vortex are highly skewed; for the proper representation of these cases, the program has been modified to treat each highly skewed panel as a pair of triangles.

The two programs are validated by comparing the chordwise pressure distribution of several blade tip planforms with experimental data. The comparison, for the most part, is good. The triangular panel representation improved the chordwise pressure distribution near the tip region for higher mean angle of attack.

9.0 REFERENCES

1. Rao, B.M. and Maskew, B., "Inviscid Analysis of Unsteady Blade Tip Flow--Correlation Studies", NASA CR-172506, 1985.

2. Maskew, B., "Prediction of Subsonic Aerodynamic Characteristics: A Case for Low-Order Panel Methods", J. Aircraft, Vol. 19, No. 2, February 19082. pp. 157-163.

3. Maskew, B., Rao, B.M and Dvorak, F.A., "Prediction of Aerodynamic Characteristics for Wings with Extensive Separations", Paper No. 31 in 'Computation of Viscous-Inviscid Interactions', AGARD-CP-291, February 1981.

4. Maskew, B., "Influence of Rotor Blade Tip Shape on Tip Vortex Shedding--An Unsteady Inviscid Analysis", Proc. 36th Annual Forum of the AHS, Paper S0-6, May 1980.

5. Summa, J.M. and Maskew, B., "A Surface Singularity Method for Rotors in Hover or Climb", USAAVRADCOM-TR-81-D-23, December 1981.

6. Clark, D.R. and Maskew, B., "An Analysis of Airframe/Rotor Interference in Forward Flight", Paper No. 50, Presented at the 7th European Rotorcraft and Powered Lift Aircraft Forum, Garmisch-Partenkirchen, FRG, September 1981.

7. Geissler, W., "Dynamic Stall Investigations on a Rectangular Blade Tip", DFVLR--Aerodynamic Institut fur Aeroelastik, IB232-82J04, June 1982.

8. Maskew, B., "Program VSAERO, A Computer Program for Calculating Computer Programs for Calculating the Non-Linear Aerodynamic Characteristics of Arbitrary Configurations", NASA CR-166476, November 1982.

9. Morino, L, Chen, L.T. and Sucio, E.O., "Steady and Oscillatory Subsonic and Supersonic Aerodynamics around Complex Configurations", AIAA J., Vol. 13, No. 3, March 1975, pp. 368-374.

10. Send, W., "Test Computations of the Unsteady Wake Integral in Incompressible Flow", DFVLR, 05 51/709-2387, February 1982.

1. Report No.	2. Government Accession No.	3. Recipient's Catalog No.
NASA CR-3868		

4. Title and Subtitle	5. Report Date
Unsteady Analysis of Rotor Blade Tip Flow	May 1985
	6. Performing Organization Code

7. Author(s)	8. Performing Organization Report No.
B. Maskew and B. M. Rao	AMI Report 8412
	10. Work Unit No.

9. Performing Organization Name and Address	11. Contract or Grant No.
Analytical Methods, Inc. 2047 - 152nd Avenue, N.E. Redmond, WA 98052	NAS1-15472
	13. Type of Report and Period Covered
12. Sponsoring Agency Name and Address	Contractor Report
NASA Langley Research Center Hampton, VA 23665	14. Sponsoring Agency Code

15. Supplementary Notes

Langley Technical Monitor: Wayne R. Mantay
Final Report

16. Abstract

The theoretical development of two computer programs, VSAERO-TS and VSAERO-H, for calculating the unsteady aerodynamic characteristics of arbitrarily shaped wings oscillating in pitch is presented. The effect of several wake parameters--wake length, the number of time steps and panel density--on chordwise pressure distribution in VSAERO-TS is presented. Also, the convergence characteristics of both programs are discussed.

In the computer programs the influence coefficient for each panel is formulated for a planar surface and so a skewed panel is represented by a projected flat quadrilateral lying in the mean plane. Panels in the extreme roll-up region of the tip vortex are highly skewed; for the proper representation of these cases the program has been modified to treat each highly skewed panel as a pair of triangles.

The two programs are validated by comparing the chordwise pressure distribution of several blade tip planforms with experimental data. The comparison, for the most part, is good. The triangular panel represenation improved the chordwise pressure distribution near the tip region for higher mean angle of attack.

17. Key Words (Suggested by Author(s))	18. Distribution Statement
Aerodynamics Unsteady Flow Harmonic Wake Time-Stepping Calculation	Unclassified - Unlimited Subject Category 02

19. Security Classif. (of this report)	20. Security Classif. (of this page)	21. No. of Pages	22. Price
Unclassified	Unclassified	56	A04

For sale by the National Technical Information Service, Springfield, Virginia 22161 NASA-Langley, 1985